Vacuum polarization energy of a soliton with many internal degrees of freedom

by

Arne du Toit

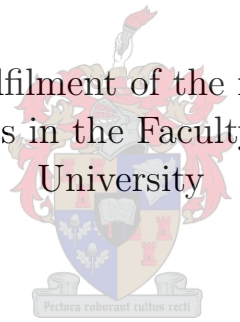

Thesis presented in partial fulfilment of the requirements for the degree of Master of Science in Physics in the Faculty of Science at Stellenbosch University

Supervisor: Prof. Herbert Weigel

April 2022

Declaration

By submitting this thesis electronically, I declare that the entirety of the work contained therein is my own, original work, that I am the sole author thereof (save to the extent explicitly otherwise stated), that reproduction and publication thereof by Stellenbosch University will not infringe any third party rights and that I have not previously in its entirety or in part submitted it for obtaining any qualification.

Date: April 2022

Abstract

The main objective of this thesis is to numerically compute the vacuum polarization energy (VPE) of solitons in a multi-component model by means of spectral methods. The VPE is the leading quantum correction to the classical energy of the soliton. We compute the classical energy of these solitons and implement the properties of scattering data to extend the calculation to the VPE. Two popular soliton models in one space dimension, the Sine-Gordon and the ϕ^4 kink, are analytically assessed and the VPEs are computed utilizing the Jost functions. Computing the VPE from the Jost function makes ample use of analytical properties of scattering data, i.e. the wave-functions in the quantum mechanical treatment of static potential scattering. We generalize that program to field theories (still in one space dimension) containing components with different masses. These techniques are used to explore the multi-component model introduced by Gani et al. In that model the stationary field equations have two soliton solutions, of which only one minimizes the classical energy. The other one is unstable. We examine and verify that scenario from the corresponding Jost functions allowing us to identify bound states with imaginary energy eigenvalues (with a relativistic dispersion relation) because their existence signals instabilities. We then compute the VPE of the stable soliton. In a certain subset of the model parameters the two solitons are classically degenerate. Our calculation of the VPE provides a definite answer to the question which of the degenerate solitons is preferred.

Uittreksel

Die hoofdoel van hierdie tesis is om die vakuumpolarisasie-energie (VPE) van solitons in 'n multi-komponent model numeries deur middel van spektraalmetodes te bereken. Die VPE is die leidende kwantumkorreksie tot die klassieke energie van die soliton. Ons bereken die klassieke energie van hierdie solitons en implementeer die eienskappe van verstrooiingsdata om die berekening na die VPE uit te brei. Twee gewilde soliton modelle in een ruimtelike dimensie, die Sine-Gordon model en die ϕ^4 kinkel, word analities geassesseer en die VPEs word bereken deur die Jost funksies te gebruik. Die berekening van die VPE vanaf die Jost funksie maak ruim gebruik van analitiese eienskappe van verstrooiingsdata, dit wil sê die golffunksies in die kwantummeganiese beskrywing van statiese potensiaalverstrooiing. Ons veralgemeen hierdie program na veldteorieë (steeds in een ruimtelike dimensie) wat komponente wat verskillende massas bevat. Hierdie tegnieke word gebruik om die multi-komponent model wat deur Gani et al. voorgestel is, te ondersoek. In daardie model het die stationêre veldvergelykings twee soliton oplossings waarvan slegs een die klassieke energie minimeer. Die ander een is onstabiel. Ons ondersoek en verifieer hierdie geval met die ooreenstemmende Jost funksies wat ons in staat stel om gebonde toestande met imaginêre energie-eiewaardes (met 'n relativistiese dispersieverband) te identifiseer aangesien hul bestaan onstabiliteite aandui. Ons bereken dan die VPE van die stabiele soliton. In 'n sekere gebied van die model parameters is die twee solitons klassiek ontaard. Ons berekening van die VPE bied 'n definitiewe antwoord op die vraag van watter van die ontaarde solitons voorkeur geniet.

Acknowledgments

I'd like to start by expressing my profound gratitude towards my supervisor, Professor Herbert Weigel. It has been an absolute honor to learn from such an esteemed physicist. He was a constant source of inspiration on the best and worst days. His guidance and patience is the entire reason I was able to persevere and complete this thesis.

Next I'd like to thank my loving parents, André and Hannelie du Toit. Their endless support throughout my life is the source of my ambition and determination. I hope to always make them proud as a minuscule token of appreciation for their continuous believe in me as a person.

My partner, Alex Herzenberg, deserves a tremendous amount of recognition for his daily support and non-stop contribution to the journey I am on to achieve my dreams. He is the driving force behind my motivation and my solid foundation in times when I feel ungrounded.

Lastly, I would like to thank the financial contributions from the Stellenbosch University physics department for providing me with a partial bursary, as well as the financial contributions of Alex to invest in my future by contributing to my study fees.

Contents

List of Figures

Chapter 1

Introduction

Quantum field theory (QFT) is the mathematical language used to describe properties and interactions of elementary particles [1][2]. The first major and successful application of QFT was Quantum electrodynamics which was developed in the 1920s originating from the work done by Paul Dirac on the quantum theory of an electron [3][4]. Relativistic QFT combines the concepts from both quantum mechanics and special relativity.

A main motivation for constructing QFTs was the shortcomings of quantum mechanics which only explains the wave properties of particles but not the particle nature of waves. QFT also overcomes the instabilities in relativistic quantum mechanics that emerge from the energy eigenvalues not being bound from below. In Ref. [5] the connection between the different fields in physics is explained as well as the shortcomings we currently face in developing a unified theory embracing electroweak and strong interactions.

In the case of nonlinear field equations, it is very likely that the theory has soliton (or solitary wave) solutions, in particular in theories with one space dimension. A solitary wave is a solution to a non-linear system of differential equations with specific characteristics which will be specified shortly. Such a solution was first described by John Scott Russell and was then referred to as a translational wave [6]. The theory was expanded on when Diederik Korteweg and Gustav de Vries studied the latter called Korteweg-De Vries (KdV) equation, which is a non-linear partial differential equation with a traveling wave solution, known as a soliton [7]. Exact solutions to the equation and modified variants thereof are widely found in the literature, see e.g. Refs. [8][9]. The most extraordinary characteristic of a soliton is that it consists of a permanent form. This form remains unchanged even when interactions with another soliton occur. The only change after the interaction holds a possible phase shift.

Nowadays solitons are found to address a number of mathematical problems across various fields in physics. A well known example arises form the non-linear Klein-Gordon field theory, commonly referred to as the ϕ^4 model. The solitary waves observed are kink solitons [10] which behave like particles under the influence of external forces [11][12]. These solitons express the domain walls in ferroelectrics [13] and ferromagnets [14], as well as the fractal structure of the cosmic domain walls [15] also observed in condensed matter physics [16]. The total energy of these solitons, which is calculated by integrating the energy density over all space, is inversely proportional to the coupling constant found in the model's Lagrangian. When combining the scaling laws of quantum chromodynamics of (the fundamental theory for the strong nuclear interaction) under the change of the number of color degrees of freedom, Witten [17] conjectured to identify baryons (proton,neutron,...) as solitons in an effective meson theory. This line of argument supports the

Skyrme model [18] with its topologically stablized solitons as a model for baryons [19]. Over the past decades this concept has been successfully applied in the description of baryons' properties. See Ref. [20] for a review of those activities.

Canonical quantization is used to make the transition from classical dynamics to quantum theory. During this process, generalized coordinates and momenta are expressed as operators. Of course in QFT these coordinates are the field fluctuations. When canonically quantizing fluctuations around the vacuum, the infinite vacuum energy can typically be eliminated by means of normal ordering.

Our interest, for this thesis, lies in the quantum corrections to soliton energies. The classical energy obviously does not include the quantum contributions from the field fluctuations about the soliton. In the case of a nonlinear field equation with a soliton solution, the fluctuations about the soliton change the vacuum energy. Imposing normal ordering with respect to the annihilation operators for fluctuations about the translationally invariant vacuum does not fully remove the vacuum energy. The remaining difference is called the vacuum polarization energy (VPE) and can be obtained by applying spectral methods. These methods examine the spectrum of the fluctuations when interacting with the soliton. This spectrum is characterized by the bound state energies and the scattering matrix. There exist exact results for the VPE for various models, including the Sine-Gordon and ϕ^4 kink model, which will also be discussed in this thesis in order to establish the machinery of spectral methods for computing the VPE of solitons. In most other cases, however, we have to resort to numerical computations.

In this thesis we examine the VPE of a multi-component model within one space dimension. The particular model was first introduced by Gani et al. [21]. Essentially the model has three parameters after rescaling to dimensionless fields and coordinates. In a subset of two parameters, analytic soliton solutions to the stationary field equations can be constructed. There are actually two sets of solutions. Which of the two solutions has the smaller classical energy depends on the particular choice of model parameters. We will compute the VPE for both cases. In particular there is a one-dimensional subset in parameter space in which the two solutions have equal classical energies. In that case the VPE is decisive for the true solution.

This thesis follows the following structure: In chapter 2 we consider a simple model of which the classical energy is calculated and the process of expanding to the VPE is described in terms of the analytical properties of the scattering data. In chapter 3 we analyse the solitons for the Sine-Gordon and ϕ^4 kink model by confirming the analytical classical energy and the VPE. Chapter 4 explores the same models described by means of the Jost function. In chapter 5 we expand on the multidimensional model introduced by Gani et al. [21] by applying the methods of chapter 4. The final (numerical) results are contained in chapter 6. We conclude and summarize in chapter 7. Appendices on the techniques of the numerical simulations are also added.

Chapter 2

VPE Calculations

2.1 Simple Model

We consider Lagrangians (or Lagrange densities $\mathcal{L}$) that are local functions of the field(s) with at most two field derivatives. We start with a simple model defined by a standard Lagrangian for scalar field theories, that contains a single real scalar field (ϕ) in one space(z) and time(t) dimensions (also indicated as $D = 1 + 1$),

$$\mathcal{L} = \frac{\lambda}{2}\dot{\phi}^2 - \frac{\lambda}{2}\phi'^2 - \frac{\lambda}{2}(\phi^2 - 1)^2, \tag{2.1}$$

with the field potential $U(\phi) = \frac{\lambda}{2}(\phi^2 - 1)^2$. Here λ is an overall factor and all fundamental physics constants are set to 1 ($c = \hbar = 1$). Originally λ was the coefficient of the non-derivative term in the Lagrangian. After appropriate rescaling of the coordinates, it turns into an overall factor that has no relevance for the (classical) field equations. However, as we will see below, it affects the canonical commutation relations and becomes a loop counting parameter. The first two terms stem from the derivative of the field with respect to space and time independently, commonly also written as

$$\partial_\mu\phi\partial^\mu\phi = \dot{\phi}^2 - \phi'^2,$$

where the dot represents the time derivative and the prime denotes the spacial derivative. In this standard Lagrangian the square of the time derivative of the field denotes the kinetic energy, whereas the remaining terms represent the potential energy. For there to exist non-trivial finite energy solutions the potential must have at least two degenerate minima [22]. With the quartic potential term, the linear theory becomes self interacting due to the Euler-Lagrange equation being non-linear. The Lagrangian describes a relativistic system that is Lorentz invariant and remains unchanged by a parity transformation.

When the extremal condition, $\frac{\partial U}{\partial \phi} = 0$, only has a single solution, $\phi(t, z) = 0$ must be at that minimum for all z. However if $U(\phi)$ has at least two minima, such as a double well potential, it is possible for one solution to be situated at $z \mapsto -\infty$, while the other can be found at $z \mapsto \infty$. This means that there may exist an energetically stable field configuration that connects these two solutions and is no longer invariant under the symmetry of translation and thus reflects spontaneous symmetry breaking.

The action (measured in units [energy·time]) of the system is determined by either a time integral over the Lagrangian or a space time integral over the Lagrange density, such that,

$$S = \int dtL = \int dtdz\mathcal{L}. \tag{2.2}$$

When Hamilton's principle, stating that the variation of the action must be zero, is applied to the action, we obtain the equation of motion. Varying the field $\phi \to \phi + \delta\phi$ and integrating by parts, the variation of the action becomes

$$\delta S = \int dt dz \delta\phi \left(\frac{\partial \mathcal{L}}{\partial \phi} - \partial_\mu \frac{\partial \mathcal{L}}{\partial(\partial_\mu \phi)} \right) = 0. \tag{2.3}$$

This must be true for any field variation $\delta\phi$, leading to the Euler-Lagrange equation

$$\frac{\partial \mathcal{L}}{\partial \phi} - \partial_\mu \frac{\partial \mathcal{L}}{\partial(\partial_\mu \phi)} = 0. \tag{2.4}$$

For stationary solutions the equation of motion for the Lagrangian in Eq. (2.1) reads

$$\phi'' - 2\phi(\phi^2 - 1) = 0. \tag{2.5}$$

It is straightforward to verify that $\phi_0 = \pm \tanh(z - z_0)$ are viable static solutions. These solutions solve a non-linear field equation with a potential energy consisting of two degenerate minima by which we interpret the solutions as solitary waves, since any localized static solution is a solitary wave [10].

Solitary waves, and their extension to solitons, are certain solutions to non-linear wave equations that retain special characteristics. There exist two requirements associated to these solutions, namely,

i. A single wave packet (solution) should retain its velocity and shape, where the retention of its shape refers to the solution being non-dispersive.

ii. Several solutions should retain the same requirements as for (i.) even after collisions.

Solutions that fulfill the first requirement are deemed solitary waves, whereas if both requirements are upheld the solution is classified as a soliton. All non-trivial finite energy solutions interpolate between two neighboring minima of the field potential $U(\phi)$. We first examine the classical energy of configurations, followed by the quantum corrections. Since the energy is central to our calculations it is worth elaborating on the simple restrictions corresponding to solitary waves and their associated energy density. The conserved energy functional will require the energy density to be integrated over all space, thus the density must approach zero sufficiently fast at spatial infinity. Furthermore, it is required to be finite away from spatial infinity.

The energy density or Hamiltonian density is the 00-component of the canonical energy momentum tensor $T^{\mu\nu}$ [23], which is defined as

$$T^{\mu\nu} = \frac{\partial \mathcal{L}}{\partial(\partial_\mu \phi)} \partial^\nu \phi - g^{\mu\nu} \mathcal{L}. \tag{2.6}$$

Thus the energy density is given by,

$$\mathcal{E}(z) = T^{00} = \frac{\partial \mathcal{L}}{\partial \dot{\phi}} \dot{\phi} - \mathcal{L} = \frac{\lambda}{2}\dot{\phi}^2 + \frac{\lambda}{2}\phi'^2 + \frac{\lambda}{2}(\phi^2 - 1)^2. \tag{2.7}$$

We can calculate the specific energy density for the static solution, ϕ_0, as,

$$\mathcal{E}(z) = \frac{\lambda}{2}\phi'^2 + \frac{\lambda}{2}(\phi^2 - 1)^2 = 2\lambda U(\phi) = \lambda \operatorname{sech}^4(z - z_0). \tag{2.8}$$

Then we obtain the total classical energy by integrating the energy density over all space,

$$E(z) = \int_{-\infty}^{\infty} dz \mathcal{E}(z) = \frac{4\lambda}{3}. \tag{2.9}$$

This calculation of the classic energy has been quite simple. The leading quantum correction is more complicated. This correction is commonly called the vacuum polarisation energy (VPE) and will be discussed in the next section.

2.2 Calculating the Vacuum Polarization Energy (VPE)

To quantise the theory we consider harmonic fluctuations about stationary configurations by expanding the Lagrangian up to quadratic order, resulting in linear field equations for these fluctuations. There are at least two stationary configurations, of which the first is the trivial vacuum ($\phi_0 = \pm 1$) and the second a soliton ($\phi_0 = \pm\tanh(z)$). Each mode carries a zero point energy $\omega_k = \sqrt{k^2 + m^2}$, where k is the wave number and labels the mode. In case of the soliton, bound states emerge, which are reflected by an imaginary wave number. The leading quantum correction to the energy of the soliton is then given by the difference of the two sets of zero point energies. For the fluctuations about the soliton this label has discrete (bound state) and continuous (scattering states) components. Normal ordering removes the zero point energies for fluctuations about one particular stationary configuration, but not both simultaneously.

We start by defining a field operator ϕ, which arises from quantizing about the trivial vacuum in the absence of the soliton, or in other words quantizing the free plane wave solution, as

$$\phi = \int \frac{dk}{2\pi(2\omega)} \left[a(k)e^{-ik\cdot z} + a^\dagger(k)e^{ik\cdot z}\right], \tag{2.10}$$

where the time derivative of this operator is

$$\dot{\phi} = -i \int \frac{dk}{2\pi(2\omega_k)} \omega_k \left[a(k)e^{-ik\cdot z} - a^\dagger(k)e^{ik\cdot z}\right]. \tag{2.11}$$

The factor of ω_k comes from the time derivative of $k \cdot z = \omega_k t - kz$. From this we obtain the canonical field momentum,

$$\Pi = \frac{\partial \mathcal{L}}{\partial \dot{\phi}} = \lambda\dot{\phi} = -i\lambda \int \frac{dk}{2\pi(2\omega_k)} \omega_k \left[a(k)e^{-ik\cdot z} - a^\dagger(k)e^{ik\cdot z}\right]. \tag{2.12}$$

The equal time canonical commutators relations for these operators are

$$[\phi(z,t), \Pi(z',t)] = i\delta(z - z') \tag{2.13}$$

$$[\phi(z,t), \dot{\phi}(z',t)] = \frac{i}{\lambda}\delta(z - z'). \tag{2.14}$$

In order to extract $a(q)$ and $a^\dagger(q)$, consider the following integral in coordinate space,

$$\begin{aligned}
&\int dz e^{iq\cdot z}\left[\omega_q\phi + i\dot{\phi}\right] \\
&= \int dz e^{iq\cdot z} \int \frac{dk}{2\pi(2\omega_k)} \left[e^{-ikz}a(k)(\omega_q + \omega_k) + e^{ikz}a^\dagger(k)(\omega_q - \omega_k)\right] \\
&= a(q),
\end{aligned} \tag{2.15}$$

since $\delta(q \pm k)$ implies $\omega_q = \omega_k$. Similarly $a^\dagger(q) = \int dz e^{-iqz}(\omega_q\phi - i\dot{\phi})$. Therefore the commutation relations between these above mentioned operators are

$$\left[a(q), a^\dagger(q')\right] = \frac{1}{\lambda} 2\pi 2\omega_q \delta(q - q'). \tag{2.16}$$

Next we establish the Hamiltonian description, for which we first need the Hamiltonian density, which we can calculate by using the equation $\mathcal{H} = \Pi\dot{\phi} - \mathcal{L}$, such that

$$\mathcal{H} = \frac{\lambda}{2}(\dot{\phi}^2 + \phi'^2 + m^2\phi^2). \tag{2.17}$$

Furthermore, the Hamiltonian is the spatial integral of the Hamiltonian density, which is computed by inserting Eqs.(2.12,2.13)

$$\begin{aligned} H = \int dz\mathcal{H} &= \lambda \int \frac{dk}{(2\pi)(2\omega_k)}\omega_k \left[a(k)a^\dagger(k) + a^\dagger(k)a(k)\right] \\ &= \lambda \int \frac{dk}{2\pi(2\omega_k)}\omega_k \left(a^\dagger(k)a(k) + \frac{1}{2\lambda}(2\pi)\omega_k 2\delta(0)\right), \end{aligned} \tag{2.18}$$

where $2\delta(0) = \frac{1}{\pi}\int dz e^{i0} = \frac{L}{\pi}$ expresses the free density of states, ρ_0, with L being the size of the one dimensional universe. The number of quantum mechanical states can be summed by solving the phase space integral, of which each phase space of size $\frac{dkdz}{2\pi}$ contains a single quantum state,

$$\frac{1}{2}\int dk\omega_k\delta(0) = \frac{1}{2}\int \frac{dkdz}{2\pi}\omega_k = \frac{1}{2}\sum_k \omega_k. \tag{2.19}$$

In order to find the spectrum of the Hamiltonian we need to calculate the commutation relations between the Hamiltonian and the creation and annihilation operators. We find that,

$$\begin{aligned} [H, a(q)] &= \lambda \int \frac{dk}{(2\pi)^2 2\omega_k}[a^\dagger a(k), a(q)] \\ &= \lambda \int \frac{dk}{2\pi 2\omega_k}\omega_k[a^\dagger(k), a(q)]a(k) \\ &= -\omega_q a(q), \end{aligned} \tag{2.20}$$

and similarly $[H, a^\dagger(q)] = \omega_q a^\dagger(q)$. Hence $a^\dagger(q)$ creates quantum states with energy $\omega_q = \sqrt{q^2 + m^2}$ and $a(q)$ annihilates these quantum states. The annihilation operator on the vacuum energy state yields zero, such that $a(q)\,|0\rangle = 0$. Next we can evaluate the VPE using the Hamiltonian, which yields,

$$\langle 0|\, H\, |0\rangle = \frac{1}{2}\sum_k \omega_k. \tag{2.21}$$

The VPE does not contain the model parameter λ, since the commutation relation between the creation and annihilation operators has a factor $\frac{1}{\lambda}$, whilst the Hamiltonian, Eq (2.17), contained the overall factor λ, causing them to cancel. When we compare the VPE to the classical energy we find,

$$\frac{\langle 0|\, H\, |0\rangle}{E_{cl}} \approx \frac{1}{\lambda}. \tag{2.22}$$

Even though the field equations for the quantum field do not contain λ, this parameter distinguishes classical and quantum contributions to the energy. It may therefore be referred to as loop-counting parameter.When reinforcing standard units this is proportional to $\hbar$.

2.3 Small-Amplitude Quantum Fluctuation

In order to obtain the VPE, we need to evaluate the spectrum of the small-amplitude oscillations about the time independent field configuration ϕ_0. We add time-dependent fluctuations, $\eta(z,t)$:

$$\phi(z,t) = \phi_0(z) + \eta(z,t) = \tanh(z) + \eta(z,t). \tag{2.23}$$

When substitute $\phi(z,t)$ into Eq. (2.5), we obtain,

$$\ddot{\eta} - \eta'' = 2\eta[1 - 3\tanh^2 z], \tag{2.24}$$

where anything higher than the leading linear order of η has been omitted. At $z \to \pm\infty$ this expansion simplifies to

$$\ddot{\eta} - \eta'' = -4\eta, \tag{2.25}$$

which precisely resembles the Klein-Gordon equation if we consider the mass squared term to be, $m^2 = 4$. It is thus suggested to rewrite the previous equation as,

$$\ddot{\eta} - \eta'' = -4\eta - 6(\tanh^2 z - 1)\eta. \tag{2.26}$$

This defines the fluctuation potential $V(z) = 6(\tanh^2 z - 1)$. We factorize η by means of the ansatz, conveniently set up such that the time dependency separates

$$\eta(z,t) = e^{-i\omega_k t}\eta_k(z). \tag{2.27}$$

If we combine this with the dispersion relation $\omega_k = \sqrt{k^2 + m^2}$ we obtain a new stationary wave equation,

$$\eta_k''(z) = -k^2\eta_k(z) + V(z)\eta_k(z), \tag{2.28}$$

for which the eigenfunctions and eigenvalues are known [10]. There exist two discrete bound state solutions, followed by the continuum $k \geq 0$. The two bound state wave-functions are

$$\eta_1(z) = \frac{1}{\cosh^2 z} \qquad \text{and} \qquad \eta_2(z) = \frac{\sinh z}{\cosh^2 z}. \tag{2.29}$$

Solving the wave equation by substituting η_1 yields $k^2 = -4$ and $\omega_k = 0$. Since ω_k signifies the frequency of the fluctuation and is equal to zero, η_1 is the wave function of the zero mode. This confirms that it does not cost additional energy when shifting ϕ_0 by the spatial translation expressed by

$$\phi_0(z - z_0) = \tanh(z - z_0) = \tanh(z) - \frac{z_0}{\cosh^2(z)} + \ldots \tag{2.30}$$

For η_2 we obtain $k^2 = -1$ and $\omega_k^2 = 3$, which further confirms the known solution.

Next we take a closer look at the scattering solutions by elaborating on one-dimensional scattering theory.

2.4 One-Dimensional Scattering Theory

This brief overview of scattering theory will assist our understanding of the application of the spectral method in the discussions to come. We once again consider a localised potential, which implies $V(z) \to 0$ as $z \to \pm\infty$, that is also symmetric, such that $V(z) = V(-z)$. The wave-function obeys a Schroedinger type equation,

$$-\frac{d^2\psi(z)}{dz^2} + V(z)\,\psi(z) = k^2\psi(z). \tag{2.31}$$

In one spatial dimension, the solutions to the Schroedinger equation merely consist of forward and backward moving plane waves, unlike in higher dimensions where the solutions have additional angular dependencies. We take a closer look at both of these cases, starting with the forward scattering solutions, for which the

wave originates from the far left (the negative $z-$axis). When this wave interacts with the potential it will either be reflected, transmitted or, being quantum mechanics, both. All these possibilities are parameterized by,

$$\psi_{\text{right}}(z) = \begin{cases} e^{ikz} + R_1 e^{-ikz} & z \to -\infty \\ T_1 e^{ikz} & z \to +\infty \end{cases} . \tag{2.32}$$

The first term, e^{ikz}, represents a plane wave originating from negative spatial infinity, moving towards the right. The next term, $R_1 e^{-ikz}$, represents the wave that has been partially reflected to an extent defined by the coefficient $R_1 \in \mathbb{C}$. The final term $T_1 e^{ikz}$ represents the fraction of the amplitude that has been transmitted, as the same exponential function as the original wave motion, since $V(\infty) = V(-\infty) = 0$. Similarly the case for which the wave originates from positive spatial infinity and propagates to the left is parametrized by,

$$\psi_{\text{left}}(z) = \begin{cases} T_2 e^{-ikz} & z \to -\infty \\ e^{-ikz} + R_2 e^{ikz} & z \to +\infty \end{cases} . \tag{2.33}$$

Here, the coefficients $R_2 \in \mathbb{C}$ and $T_2 \in \mathbb{C}$ serve the same purpose, to indicate the magnitude of the backward moving wave, that is reflected and transmitted respectively. Furthermore, the probability of reflection and transmission are the respective absolute squares,

$$R = |R_i|^2 \quad \text{and} \quad T = |T_i|^2, \tag{2.34}$$

where $i = 1, 2$. Space and time reflection symmetry yield $R_1 = R_2$ and $T_1 = T_2$. From current conservation [1] it follows that the probability of a wave being reflected and transmitted should sum to one, such that,

$$R + T = 1.$$

From the reflection and transmission amplitudes we construct the scattering (or S-) matrix,

$$S(k) = \begin{pmatrix} T_1 & R_1 \\ R_2 & T_2 \end{pmatrix}. \tag{2.35}$$

The sum $R + T = 1$ translates into a unitary scattering matrix.

Since $V(z) = V(-z)$, the solutions decouple into symmetric $\psi_+(z)$ and antisymmetric $\psi_-(z)$ channels. These wave-functions obey $\psi_\pm(z) = \pm\psi_\pm(-z)$. It is thus obvious that it is sufficient to construct them explicitly for $z \geq 0$. Since they decouple, the asymptotic conditions for the scattering solutions are as simple as

$$\psi_\pm(z) \approx e^{-ikz} \pm S_\pm(k) e^{ikz}, \tag{2.36}$$

with sign conventions such that the scattering matrix $S_\pm = 1$ when $V(z) = 0$. Current conservation implies $|S_\pm|^2 = 1$ and we can parametrize $S_\pm = e^{2i\delta_\pm(k)}$, where $\delta_\pm(k)$ are the real phase shifts in the symmetric and antisymmetric channels. In actual calculations we will extract the phase shifts from the boundary conditions $\psi'_+(0) = 0$ and $\psi_-(0) = 0$. Asymptotically at, $z \to +\infty$, we have $\psi_+ \sim \cos(kz + \delta_+)$ and $\psi_- \sim \sin(kz + \delta_-)$.

2.4.1 Scattering Solutions Concerning the Simple Model

We want to obtain solutions to the wave equation of Eq. (2.31) with the specific boundary conditions just mentioned. Let's consider the ansatz $\psi = A_k(z) e^{ikz}$ with asymptotic condition $\lim_{z\to\infty} A_k(z) = 1$, which

[1] The current is $J_\mu = \frac{1}{2i}(\psi^* \partial_\mu \psi - \psi \partial_\mu \psi^*)$ and conservation means $\partial_\mu J^\mu = 0$.

yields the following differential equation,

$$A_k^{''}(z) = -2ikA_k^{'}(z) + V(z)A_k(z). \tag{2.37}$$

Since the equation for ψ is real, $\psi^*(z) = A_k^*(z)e^{-ikz}$ is also a solution. This combined with the boundary condition gives $A_k^*(z) = A_{-k}(z)$. This behavior is exactly like that of a Jost solution, to be discussed in later sections. We can analytically calculate the solution [10] for the potential in Eq. (2.26),

$$A_k(z) = N[3\tanh^2 z - 1 - k^2 - 3ik\tanh z], \tag{2.38}$$

with normalization constant N. By implementing the asymptotic conditions, we can calculate this constant as,

$$N = \frac{1}{2 - k^2 - 3ik}. \tag{2.39}$$

The scattering solutions in the symmetric and antisymmetric channel are obtained as,

$$\psi_\pm(z) = A_k^*(z)e^{-ikz} \pm A_k(z)e^{ikz}S_\pm. \tag{2.40}$$

The S-matrix elements are calculated by considering the boundary conditions for each channel respectively. For the antisymmetric channel, the boundary condition is simply $\psi_-(0) = 0$, which yields,

$$S_- = \frac{A_k^*(0)}{A_k(0)} = \frac{N^*}{N}\frac{-1-k^2}{-1-k^2} = \frac{N^*}{N} = \frac{2-k^2-3ik}{2-k^2+3ik}. \tag{2.41}$$

For the symmetric channel, the calculation is slightly more complicated since the boundary condition involves the derivative of the wave function, $\psi_+^{'}(0) = 0$, which leads to the corresponding S-matrix element,

$$S_+ = \frac{ikA_k^*(0) - A_k^{*'}(0)}{ikA_k(0) + A_k^{'}(0)} = \frac{N^*}{N}\frac{ik(-1-k^2-3)}{ik(-1-k^2-3)} = \frac{N^*}{N} = S_-. \tag{2.42}$$

This result is due to $A^{'}(0) = -3ikN$ and $A^{'*}(0) = 3ikN^*$. In the previous section we have seen that the S-matrix can be parametrized as $S_\pm = e^{2i\delta_\pm(k)}$, from which we can obtain the phase shifts $\delta_\pm(k)$ as,

$$\tan\delta_+ = \tan\delta_- = \frac{-3k}{2-k^2} = \frac{3k}{k^2-2}. \tag{2.43}$$

The (anti)symmetric wave functions can be linearly combined to match the asymptotic conditions in Eqs. (2.32) and (2.33). This yields $T_i = \frac{1}{2}(S_+ + S_-)$ and $R_i = \frac{1}{2}(S_+ - S_-)$. Obviously $R_i = 0$, which shows that the scattering potential is reflectionless.

2.5 Analytical Properties of Scattering Data

We start from the mode sum in Eq. (2.21) for the vacuum polarization energy and subtract the free energies (the case without the presence of the potential). This yields the previously mentioned difference in energies,

$$\Delta E = E - E^{(0)} = \sum_k \frac{1}{2}\omega_k - \sum_k \frac{1}{2}\omega_k^{(0)}. \tag{2.44}$$

There are two problems associated with this difference of sums. Firstly, the first sum's modes consist of both discrete bound states and a continuum of scattering states, and secondly, neither of the sums nor their difference is finite. We will have to carefully eliminate the divergence as to provide a physical meaning. We incorporate the continuum of scattering states by discretizing the spectrum and subsequently establish the density of states for the continuum limit.

2.5.1 Correlation Between Density of States and Phase Shifts

The reason behind considering densities of states is that the difference between the density of states in the presence of a potential and the free density of states can be easily expressed by scattering data. Let us consider the small oscillation wave functions $\phi_k(z)$ that obey the relativistic wave equation,

$$\left(-\frac{d^2}{dz^2}+V\left(z\right)\right)\phi_k\left(z\right)=k^2\phi_k\left(z\right), \tag{2.45}$$

where $V(z)$ represents a typically symmetric in $(z\rightarrow -z)$ potential and $k^2=\omega_k^2-m^2$ from the dispersion relation. We only consider the antisymmetric channel (whilst the symmetric channel will be included in the final calculation) where $\phi_k(0)=0$ and the obvious solution to the free case is simply $\phi_k^{(0)}(z)=\sin\left(kz\right)$. We assume that $V(z)\rightarrow 0$ for $z\rightarrow\infty$ and that our solution to the wave equation will tend to the free solution, with a possible phase shift [24],

$$\phi_k\left(z\right)\sim\sin\left(kz+\delta\left(k\right)\right)\qquad\text{for large}\quad z. \tag{2.46}$$

The phase shift is represented by $\delta(k)$ and as indicated, only depends on k. We need to enforce some additional conditions in order for our solutions to the wave equation to be enumerable. We prescribe the boundary condition $\lim_{z\rightarrow L}\phi_k\left(z\right)=0$, so that our solutions for $\sin\left(kL+\delta(k)\right)=0$ induces a discrete spectrum of allowed values for k. The length scale L is much larger than the range of the potential, such that Eq. (2.46) holds. The boundary condition is solved by,

$$\pi n(k)=kL+\delta\left(k_n\right)\quad\text{or}\quad n(k)=\frac{1}{\pi}\left(kL+\delta\left(k_n\right)\right). \tag{2.47}$$

This last equation means that $n(k)$ is the number of states with wave number less than or equal to k. From this we find the density of states as $\rho\left(k\right)=\frac{dn}{dk}=\frac{1}{\pi}\left(L+\frac{d\delta(k)}{dk}\right)$. The case without the potential has $\delta(k)=0$. Hence the difference of the density of states does not depend on L,

$$\Delta\rho\left(k\right)=\rho\left(k\right)-\rho^{(0)}\left(k\right)=\frac{1}{\pi}\frac{d\delta\left(k\right)}{dk}, \tag{2.48}$$

and therefore equals the continuum limit $L\rightarrow\infty$. We translate our findings for the density of states back to the mode sum by replacing the sum by the integral,

$$\begin{aligned}\Delta E=\frac{1}{2}\sum_k\omega_k-\frac{1}{2}\sum_k\omega_k^{(0)}&=\frac{1}{2}\sum_j^{b.s.}\omega_j+\frac{1}{2}\int_0 dk\sqrt{k^2+m^2}\Delta\rho\left(k\right)\\&=\frac{1}{2}\sum_j^{b.s.}\omega_j+\int_0\frac{dk}{2\pi}\sqrt{k^2+m^2}\frac{d\delta}{dk},\end{aligned} \tag{2.49}$$

where the sum on the right hand side is the contribution from the bound states. If we still only consider the anti-symmetric channel, we can combine this with Levinson's theorem, which relates the number of bound states ($n_{b.s.}$) of a potential difference of the phase shifts of zero and infinite wave number,

$$\delta(0)-\delta(\infty)=n_{b.s.}\pi. \tag{2.50}$$

This implies,

$$n_{b.s.}+\int_0^\infty dk\Delta\rho\left(k\right)=0 \tag{2.51}$$

which means that the difference between the number of continuum states in the free and interacting cases is accounted for, precisely, by the number of bound states. There is a slight difference when considering the symmetric channel, which will be addressed later.

We can then express the vacuum polarization energy in terms of binding energies using

$$\sum_j^{b.s.} 1 + \int_0^\infty dk \frac{d\delta(k)}{\pi dk} = 0 \tag{2.52}$$

as

$$\begin{aligned}\Delta E &= \frac{1}{2}\sum_j^{b.s.}(\omega_j - m) + \int_0 \frac{dk}{2\pi}[\sqrt{k^2+m^2} - m]\frac{d\delta(k)}{dk}\Big|_{\text{ren.}} \\ &= \frac{1}{2}\sum_j^{b.s.}(\omega_j - m) - \int_0 \frac{dk}{2\pi}\frac{k}{\sqrt{k^2+m^2}}\delta(k)\Big|_{\text{ren.}}\end{aligned} \tag{2.53}$$

where $\delta(k) = \delta_-(k) + \delta_+(k)$ contains the phase shifts of both channels. However, we still need to specify $'ren'$ as a prescription to handle the large k divergence. For this we need a better understanding of some of the techniques, as well as background on the Jost function, which will soon feature in our integral.

2.5.2 Jost Function

Jost solutions for the wave equation asymptotically approach plane waves (or possibly cylindrical or spherical waves in higher dimensions). In contrast to the (regular) scattering solutions they may be singular in two and more spatial dimensions. The regular solution is the linear contribution of the Jost solutions without singularities. The corresponding expansion coefficients are the Jost functions. They can either be computed from appropriate Wronskians or be extracted from the regularity condition for the regular solution. The Jost functions then contain the scattering phase. Yet, when generalizing the wave equation to complex wave numbers, a variety of properties can be used to simplify and/or gain deeper understanding of the VPE expressed by scattering data, Eq. (2.53). In the following we list these properties without proof (for details see Ref. [25]): for the Jost function $F(k)$, associated with an out going wave:

- For $\text{Im}(k) \geq 0$ in the complex plane, the Jost function is analytic.
- The bound state solutions are represented by simple zeroes for purely imaginary k-values ($\text{Re}\,(k) = 0$).
- For real k: $F(k) = |F(k)|e^{i\delta(k)}$ and since $|F(k)| = |F(-k)|$ and $\delta(k) = -\delta(-k)$ we have the symmetric property $F(-k) = F^*(k)$; as seen in Section 2.4.1 for scattering solutions.
- The Jost function approaches unity as $|k| \to \infty$ everywhere in the upper half complex plane. This implies that $\lim_{k\to\infty}\delta(k) = 0$.

We will expand on the Jost function in a later section when we consider a system with multiple fields with different momenta and masses.

2.5.3 Renormalisation

In quantum field theory the bare classical lagrangian does not produce finite Green's functions, requiring the implementation of renormalisation, which adds counterterms in order to cancel these divergences. The

counterterms get added at the very beginning to the bare Lagrangian and are of higher order in the loop counting parameter. Thus they are relevant to the quantum but not the classical energy. This means that the last equation stated for the vacuum polarisation energy is completed by the addition of counterterm contributions,

$$\Delta E = \frac{1}{2}\sum_{j}^{b.s}(\omega_j - m) + \int_0^\infty \frac{dk}{2\pi}\frac{k}{\sqrt{k^2+m^2}}\delta(k) + E_{CT}. \tag{2.54}$$

Still this expression is only formal, because the $k \to \infty$ singularitites must be related to (and compensated by) the singularities in E_{CT}.

2.5.4 Born Approximation

After properly defining what the calculation of the VPE integral entails, we require exact tools to regularize the divergences in the $k-$integral of Eq. (2.54) as well as in E_{CT}. Subsequently these divergences must be unambiguously removed in the renormalization process. One of these tools is the use of the Born approximation. The divergence arises from the integrand going like $1/k$ for large k. The counterterm in the lagrangian is proportional to $\phi^2 - 1$ to keep the field's vacuum expectation value unchanged by quantum effects. When substituting the soliton $\phi_0(z)$, this yields $E_{CT} = -c\int_{-\infty}^{\infty} dz V(z)$, where the contant coefficient is typically determined by dimensional regularization of the tadpole diagram, cf. subsection 2.5.5. Since this diagram is local (i.e independent of external momenta), the cancellation can be made without leaving a finite leftover (see below). This is the so-called no-tadpole renormalization scheme, which motivates to single out the contribution in Eq. (2.54) that is linear in the potential. This is the Born approximation $\delta^{(1)}(k)$ to the phase shift, which also governs its large $k-$behavior. We write the Born approximation to the VPE as

$$\Delta E^{(1)} = -\int_0 \frac{dk}{2\pi}\frac{k}{\sqrt{k^2+m^2}}\delta^{(1)}(k). \tag{2.55}$$

The Born approximation applies to the sum of the phase shifts of the symmetric and antisymmetric channels:

$$\text{Antisymmetric} : \delta_-^{(1)}(k) = -\frac{1}{2k}\int_{-\infty}^{\infty} dz V(z)\sin^2(kz) \tag{2.56}$$

$$\text{Symmetric} : \delta_+^{(1)}(k) = -\frac{1}{2k}\int_{-\infty}^{\infty} dz V(z)\cos^2(kz) \tag{2.57}$$

$$\text{Born Approximation} : \delta^{(1)}(k) = \delta_-^{(1)}(k) + \delta_+^{(1)}(k) = -\frac{1}{2k}\int_{-\infty}^{\infty} dz V(z) \tag{2.58}$$

In section 2.5.1 we mentioned that we will include the symmetric channel in our final contribution, but not show the full derivation. This is due to the contribution of the symmetric channel being very similar to that of the antisymmetric channel, but the calculation of the phase shift is slightly more involved due to the $\phi'(0) = 0$ boundary condition. The addition of the symmetric and antisymmetric phase shifts (denoted by the Born approximation in Eq. (2.58)) is the expectation value of the potential. The Born approximation stems entirely from the continuum and does not contain any bound states. The Born approximation is the leading term from the perturbation expansion for wave-functions about the translationally invariant vacuum. These are plane waves but not bound states.

Next we can subtract the Born approximation from the scattering contributions contained in the integral in order to improve the convergence of the integral. We then add it back in as the Feynmann diagram with a single insertion of the potential $V(z)$, which is the tadpole diagram. The Feynman diagrams do not

distinguish between the symmetric and antisymmetric channel, making it crucial for the Born approximation to contain both. This yields the renormalized VPE,

$$\Delta E = \frac{1}{2}\sum_j(\omega_j - m) - \frac{1}{2\pi}\int_0^\infty \frac{k}{\sqrt{k^2+m^2}}\left(\delta(k) - \delta^{(1)}(k)\right)dk + E_{FD} + E_{CT}. \tag{2.59}$$

2.5.5 Feynman Diagrams

The VPE can formally be computed as a infinite sum of Feynman diagrams. These are the one-loop diagrams shown in Fig.[2.1]

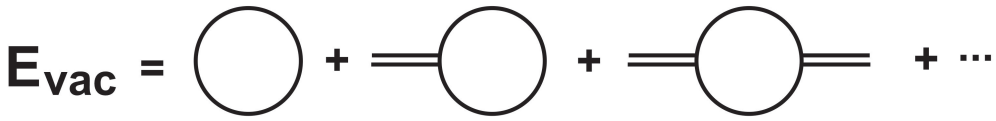

Figure 2.1: One-Loop Diagrams. Single lines represent the quantum fluctuations, while double lines denote insertions of the scattering potential.

The first diagram represents what is commonly known as the cosmological constant and does not depend on the potential at all (no insertion). The sum of the energies in the free case, $\frac{1}{2}\sum_k \omega_k^{(0)}$, is represented by this diagram. The diagrams following all consist of one loop and an increasing number of insertions from the background potential in momentum space. Only a finite number of diagrams are divergent, and in one space dimension, only that with a single insertion has ultra-violate infinities. The first diagram with a single insertion is a one-loop diagram consisting of a propagator that connects back into its original vertex and is referred to as the tadpole diagram. The integral corresponding to this diagram is,

$$E_{FD} = \frac{1}{2}\int \frac{d^2k}{(2\pi)^2}\frac{1}{k^2 - m^2 + i\epsilon}\tilde{V}(0), \tag{2.60}$$

where $\tilde{V}(0)$ is the Fourier transform of the potential at zero momentum,

$$\tilde{V}(0) = \int dz e^{i\mathbf{0}z}V(z) = \int dz V(z). \tag{2.61}$$

We see that E_{FD} is proportional to the spatial integral of $\phi^2 - 1$ with the soliton substituted. This is exactly the counterterm so that $E_{FD} + E_{CT} = 0$ is a legitimate renormalization condition. This means that the fully renormalized VPE is given by,

$$\Delta E = \frac{1}{2}\sum_j^{b.s.}(\omega_j - m) - \frac{1}{2\pi}\int_0^\infty \frac{k}{\sqrt{k^2+m^2}}\left(\delta(k) - \delta^{(1)}(k)\right)dk. \tag{2.62}$$

Chapter 3

Examples: sine-Gordon and ϕ^4 Kink

3.1 Sine-Gordon

In this section we will review the physical theory of sine-Gordon solitons.

3.1.1 Classical

We start from the bare Lagrangian for a single scalar field $\phi(z,t)$ in $(1+1)$ dimensions as,

$$\mathcal{L} = \frac{1}{2}\partial_\mu\phi\partial_\mu\phi - U(\phi), \tag{3.1}$$

where $U(\phi) = 1-\cos(\phi)$. When written in terms of physical mass (m) and coupling constant (λ), the Lagrangian becomes,

$$\mathcal{L} = \frac{1}{2}\partial_\mu\phi\partial_\mu\phi - \frac{m^4}{\lambda}\left[1-\cos\left(\frac{\sqrt{\lambda}}{m}\phi\right)\right]. \tag{3.2}$$

This Lagrangian resembles the Klein-Gordon theory when expanded in powers of the coupling constant λ,

$$\mathcal{L} = \frac{1}{2}\partial_\mu\phi\partial^\mu\phi - \frac{1}{2}m^2\phi^2 + \frac{\lambda}{4!}\phi^4 - \frac{\lambda^2}{6!}\frac{1}{m^2}\phi^6 + ... \tag{3.3}$$

though, we will remain focussed on the full Lagrangian in Eq. (3.2). From the Lagrangian we can derive the equation of motion,

$$-\frac{m^3}{\sqrt{\lambda}}\sin\left(\frac{\sqrt{\lambda}}{m}\phi\right) - \partial_\mu\partial^\mu\phi = 0. \tag{3.4}$$

For the sake of simplicity we change to dimensionless variables as follows

$$\tilde{z} = mz, \qquad \tilde{t} = mt \qquad \text{and} \qquad \tilde{\phi} = \frac{\sqrt{\lambda}}{m}\phi, \tag{3.5}$$

which leads to the simplified equation of motion,

$$\partial_\mu\partial^\mu\tilde{\phi} = -\sin\tilde{\phi}. \tag{3.6}$$

In order to express the energy density we compute the Noether charge with respect to the time translation symmetry,

$$\mathcal{E}(z) = T^{00} = \frac{m^3}{\lambda}\left[\frac{1}{2}\dot{\phi}^2 + \frac{1}{2}\phi'^2 + 1 - \cos\phi\right], \tag{3.7}$$

of which the integral over all space is the classical energy. The energy density vanishes at the minima, which can be found at $\tilde{\phi} = 2N\pi$ where $N \in \mathbb{Z}$. We obtain the static solution by calculating the following integral, which expresses a soliton centered at x_0,

$$\tilde{z} - \tilde{z}_0 = \pm \int_{\tilde{\phi}(\tilde{z}_0)}^{\tilde{\phi}(\tilde{z})} \frac{d\phi}{\sqrt{2U(\phi)}} = \pm \int_{\tilde{\phi}(\tilde{z}_0)}^{\tilde{\phi}(\tilde{z})} \frac{d\phi}{2\sin\phi/2} = \ln\tan\left(\frac{\phi}{4}\right)\Big|_{\tilde{\phi}(\tilde{z}_0)}^{\tilde{\phi}(\tilde{z})}. \tag{3.8}$$

This yields the static solutions (soliton and anti-soliton respectively) as,

$$\tilde{\phi}_{SG}(\tilde{z}) = \pm 4 \arctan\left[\exp\left(\tilde{z} - \tilde{z}_0\right)\right]. \tag{3.9}$$

taking $\tilde{\phi}(\tilde{z}_0) = \pm 1$. Using physical variables this becomes,

$$\phi_{SG}(z) = \frac{4m}{\sqrt{\lambda}} \arctan\left[e^{m(z-z_0)}\right]. \tag{3.10}$$

Both the soliton and anti-soliton have the classical energy

$$\mathrm{E}_{cl}[\phi] = \frac{8m^3}{\lambda}, \tag{3.11}$$

obtained from integrating the energy density with the static solution substituted. Note that the loop counting parameter is now λ. The number of loops is the power with which λ appears plus one.

3.1.2 Fluctuations

We consider the fluctuations $\phi(z,t) = \phi_{SG}(z) + \eta(z,t)$ around the Sine-Gordon solution set out in Ref. [26]. To linear order the field equation is,

$$\partial_\mu \partial^\mu \eta(z,t) - m^2 \eta(z,t) \cos\left[\frac{\sqrt{\lambda}}{m}\phi_{SG}(z)\right] = 0. \tag{3.12}$$

The soliton is static and we may therefore separate $\eta(z,t) = \eta(z)e^{-i\omega t}$. This yields the stationary wave equation:

$$\left[-\partial_z^2 \eta(z) + m^2\left(1 - \frac{2}{\cosh^2 mz}\right)\eta(z) = \omega^2 \eta(z)\right], \tag{3.13}$$

where we set $z_0 = 0$. It is straightforward to verify that the zero mode solution ($\omega = 0$),

$$\eta_0(z) = \sqrt{\frac{m}{2}}\frac{1}{\cosh mz}, \tag{3.14}$$

arises from translational invariance as $\eta_0(z) \sim \phi'_{SG}$. For the continuum with $\omega_k = \sqrt{k^2 + m^2}$, we obtain [27],

$$\eta_k(z) = \frac{m}{\omega_k} e^{ikz}\left(\tanh mz - i\frac{k}{m}\right). \tag{3.15}$$

We will construct the Jost solution from Eq. (3.15) in section 4.2.1.

3.1.3 Results for renormalised VPE

We need to calculate the Born approximation for the phase shift. We know that we have symmetric and antisymmetric solutions since the potential in Eq. (3.13) is symmetric under spatial reflection. Furthermore

this equation is real and since $\eta_k(-z) = -\eta_k^*(z)$ we can construct the symmetric and antisymmetric solutions explicitly,

$$\eta_+(z) = \frac{1}{2i}[\eta_k(z) - \eta_k(z)^*] \qquad \eta_-(z) = \frac{1}{2}[\eta_k(z) + \eta_k(z)^*]. \tag{3.16}$$

Asymptotically ($z \to \infty$) these combinations are proportional to $e^{-ikz} \pm S_\pm(k)e^{ikz}$, as shown by the symmetric channel expansion,

$$\eta_+(z) \sim \frac{1}{2}[e^{ikz}(1 - i\frac{k}{m}) - e^{-ikz}(1 + i\frac{k}{m})] = -\frac{1}{2}(1 + i\frac{k}{m})[e^{-ikz} + \frac{k + im}{k - im}e^{ikz}], \tag{3.17}$$

where scattering matrix is then given by

$$S_+(k) = \frac{k + im}{k - im} = \frac{|k + im|}{|k - im|}\frac{e^{i \arctan(m/k)}}{e^{-i \arctan(m/k)}}. \tag{3.18}$$

Parametrizing the scattering matrix in terms of the phase shifts $S_+(k) = e^{2i\delta_+(k)}$ and noting the opposite sign for the antisymmetric combination is compensated by the definition of S_- yields,

$$\delta_+(k) = \delta_-(k) = \arctan\left(\frac{m}{k}\right). \tag{3.19}$$

The potential is extracted from Eq. (3.13) as,

$$V(z) = -\frac{2m^2}{\cosh^2 mz}, \tag{3.20}$$

which enters the calculation of the full Born approximation, resulting in

$$\delta_+^{(1)}(k) + \delta_-^{(1)}(k) = -\frac{1}{k}\int_0^\infty dz V(z) = \frac{2m}{k}. \tag{3.21}$$

To bypass eventual jumps in the definition of $\arctan(\frac{m}{k})$ we integrate by parts,

$$\begin{aligned}
&\int_0^\infty \frac{kdk}{\sqrt{k^2 + m^2}}\left(\arctan\left(\frac{m}{k}\right) - \frac{m}{k}\right) \\
&= m\int_0^\infty dq\left(\frac{d}{dq}[\sqrt{q^2 + 1} - 1]\right)\left(\arctan\left(\frac{1}{q}\right) - \frac{1}{q}\right) \\
&= m\int_0^\infty dq(\sqrt{q^2 + 1} - 1)\left[\frac{1}{q^2 + 1} - \frac{1}{q^2}\right] \\
&= m\left(1 - \frac{\pi}{2}\right)
\end{aligned} \tag{3.22}$$

Collecting pieces yields,

$$\Delta E = -\frac{m}{2} - \frac{m}{\pi}\left(1 - \frac{\pi}{2}\right) = -\frac{m}{\pi}, \tag{3.23}$$

where the first term in the middle equation is the zero mode contribution.

3.2 ϕ^4 Kink

3.2.1 Classical

Before this brief discussion on the kink and anti-kink of the ϕ^4 model, it is worth noting that these solutions are solitary waves and not solitons. This is due to the fact that after colliding, the kink and anti-kink do not maintain their shapes and momenta, thus not upholding the second requirement mentioned in the first chapter. Nevertheless it is customary to call these configurations solitons.

Consider the typical Lagrangian used for the calculations corresponding to the ϕ^4 kink in Ref. [10],

$$\mathcal{L} = \frac{1}{2}\partial_\mu\phi\partial^\mu\phi - \frac{\lambda}{4}\left(\phi^2 - \frac{m^2}{2\lambda}\right)^2. \tag{3.24}$$

Static configurations are subject to the equation of motion,

$$\phi'' = -\frac{m^2}{2}\left(\phi - \frac{2\lambda}{m^2}\phi^3\right). \tag{3.25}$$

It is straightforward to verify that $\phi(z) = \pm\frac{m}{\sqrt{2\lambda}}\tanh\left(\frac{m}{2}(z - z_0)\right)$ are solutions to Eq. (3.25). These are the kink and antikink solitons of the ϕ^4 theory. Again, z_0 refers to the center of the soliton. These solutions connect the two vacuum solutions at $\phi_0 = \pm\frac{m}{\sqrt{\lambda}}$, which are the two degenerate minima of $V(\phi)$. Next we find the energy density for these solutions,

$$\mathcal{E}(z) = 2V(\phi) = \left(\frac{m^4}{8\lambda}\right)\operatorname{sech}^4\left(\frac{m}{2}(z - z_0)\right), \tag{3.26}$$

which, when integrated over all space yields the classical energy as,

$$E_{cl}(z) = \int_{-\infty}^{\infty} dz\mathcal{E}(z) = \frac{m^3}{3\lambda}. \tag{3.27}$$

Noticeable symmetries include translational invariance as a shift by z_0 simply translates the solution in space and the sign invariance under either a $z \to -z$ or a $\phi \to -\phi$ transformation is apparent from,

$$\phi_K(z) = -\phi_{\bar{K}}(z) = \phi_{\bar{K}}(-z). \tag{3.28}$$

3.2.2 Fluctuations

We expand the ϕ^4 kink wave equation about our static solution by considering fluctuations about it. We introduce them as,

$$\phi(z) = \phi_K(z) + \eta(z,t). \tag{3.29}$$

Again, the time dependence can be separated such that $\eta(z,t) = e^{-i\omega t}\eta(z)$. The corresponding stationary wave equation is obtained by expanding Eq. (3.25) to linear order as in Ref. [26],

$$\left[-\frac{\partial^2}{\partial z^2} - m^2 + \frac{3m^2}{2}\operatorname{sech}^2\left(\frac{m}{2}z\right)\right]\eta(z) = \omega^2\eta(z). \tag{3.30}$$

The solutions for the discrete levels are,

$$\omega_0 = 0 \qquad \text{with} \qquad \eta_0(z) = \sqrt{\frac{3m}{4}}\frac{1}{\cosh^2\left(\frac{m}{2}z\right)} \tag{3.31}$$

$$\omega_1 = \frac{\sqrt{3}m}{2} \qquad \text{with} \qquad \eta_1(z) = \sqrt{\frac{3m}{2}}\frac{\sinh\left(\frac{m}{2}z\right)}{\cosh^2\left(\frac{m}{2}z\right)}, \tag{3.32}$$

and those associated with the continuum ($\omega = \sqrt{k^2 + m^2}, k > 0$) are,

$$\eta_k(z) = Ne^{ikz}\left[-\frac{3}{2}\tanh^2\left(\frac{m}{2}z\right) + \frac{1}{2} + \frac{2k^2}{m^2} + 3i\frac{k}{m^2}\tanh\left(\frac{m}{2}z\right)\right], \tag{3.33}$$

which we have already seen in subsection (2.4.1).

3.2.3 Results for the renormalised VPE

We repeat the phase shifts from subsection (2.4.1)

$$\delta_-(k) = \delta_+(k) = \arctan\left(\frac{3mk}{2k^2 - m^2}\right). \tag{3.34}$$

The first Born approximation is

$$\delta_-^{(1)}(k) + \delta_+^{(1)}(k) = \frac{1}{k}\int_0^\infty dk \frac{3m^2}{2}\operatorname{sech}^2\frac{mx}{2} = \frac{3m}{k}. \tag{3.35}$$

Again, we integrate by parts to avoid jumps brought forth by the phase shift, $\arctan\left(\frac{3mk}{2k^2-m^2}\right)$,

$$\begin{aligned}
&\int_0^\infty dk(\sqrt{k^2+m^2}-1)\frac{d}{dk}\left(\arctan\left(\frac{3mk}{2k^2-m^2}\right) - \frac{3m}{2k}\right) \\
&\quad = m\int_0^\infty (\sqrt{k^2+1}-1)\left[\frac{1}{1+\left(\frac{3k}{2k^2+1}\right)^2}\left(\frac{3}{2k^2-1} - \frac{12k^2}{(2k^2-1)^2}\right) + \frac{3}{2k^2}\right] \\
&\quad = 3m\int_0^\infty dk(1-\sqrt{k^2+1})\left[\frac{2k^2+1}{4k^4+5k^2+1} - \frac{1}{2k^2}\right] \\
&\quad = -\frac{3m}{2} + \left(1 - \frac{\sqrt{3}}{6}\right)\pi m
\end{aligned} \tag{3.36}$$

When adding the bound state contributions we find the VPE,

$$\Delta E = m\left(\frac{1}{4\sqrt{3}} - \frac{3}{2\pi}\right). \tag{3.37}$$

Chapter 4

VPE from Imaginary Momenta

In section 2.5 we argued that it is efficient to compute the VPE as an integral over imaginary momenta because it makes redundant the determination of the bound state energies. We will verify this method for the kink and Sine-Gordon soliton.

4.1 Jost Function/Solutions for Sine-Gordon and the ϕ^4 Kink

As a first step we need to find the Jost solutions and functions. This will proceed via the Wronskian (determinant) for two differentiable functions f and g,

$$W(f,g) = f'g - fg', \tag{4.1}$$

where the primes denote the derivative with respect to the space coordinate. The Jost solutions to the wave equation have the asymptotic behaviors,

$$\lim_{z\to\infty} f_{\pm}(k,z)e^{\pm ikz} = 1, \tag{4.2}$$

and, as mentioned in section 2.5.2, have the symmetry property for real k that $f_+ = f_-^*$, since the wave equation is real. The regular solution, $\varphi(k,z)$, is a linear combination of these Jost solutions with $k-$independent boundary conditions. We start by considering the symmetric channel. The corresponding boundary conditions are,

$$\varphi(k,0) = 1 \qquad \text{and} \qquad \varphi^{'}(k,0) = 0, \tag{4.3}$$

and we write the linear combination as,

$$\varphi(k,z) = \frac{1}{2}[F_-(k)f_+(k,z) + F_+(k)f_-(k,z)], \tag{4.4}$$

where $F_-(k)$ and $F_+(k)$ refer to the Jost functions. In the non-interacting case we have $\varphi^{(0)}(x) = \cos(kx)$ and the Jost functions are $F_{\pm}^{(0)} = 1$. In order to solve for the Jost function we note that,

$$W(\varphi, f_+) = \frac{1}{2}F_+W(f_-, f_+). \tag{4.5}$$

Since the Wronskian $W(f_-, f_+)$ is space independent for solutions to wave equations without derivative interactions we simply compute it at spatial infinity: $W(f_-, f_+) = -2ik$. From this we find that,

$$F_+(k) = \frac{i}{k}W(\varphi, f_+). \tag{4.6}$$

Furthermore, we can express the Jost function in terms of the boundary conditions by evaluating the Wronskian in Eq (4.6) at $x = 0$, using Eq. (4.3),

$$W(\varphi, f_+) = \left[\varphi^{'} f_+ - \varphi f_+^{'}\right] \Big|_{x=0} = -f_+^{'}(k, 0). \tag{4.7}$$

Thus the Jost function for the symmetric channel is obtained as,

$$F_+(k) = \frac{1}{ik} f_+^{'}(k, 0). \tag{4.8}$$

Similarly we can find the Jost function for the antisymmetric channel starting with the boundary conditions,

$$\varphi(k, 0) = 0 \qquad \text{and} \qquad \varphi^{'}(k, 0) = 1. \tag{4.9}$$

The regular solution, given by

$$\varphi(k, z) = \frac{1}{2ik}[G_-(k) f_+(k, z) - G_+(k) f_-(k, z)], \tag{4.10}$$

with Jost functions $G_\pm(k)$, corresponds to the free solution of the wave equation in the antisymmetric channel $\phi^{(0)}(z) = \sin kz$. The coefficient in Eq. (4.10) again ensures that the free Jost functions equal unity. The Wronskian of the regular solution and the Jost solution yields the Jost function in the same way as above,

$$W(\varphi, f_+) = \frac{1}{2ik}(-G_+) W(f_-, f_+) = \frac{-G_+}{2ik}(-2ik) = G_+(k). \tag{4.11}$$

Once again we consider the same Wronskian and evaluate it with the boundary conditions at $x = 0$,

$$W(\varphi, f_+) = \left[\varphi^{'} f_+ - \varphi f_+^{'}\right] \Big|_{x=0} = f_+(k, 0), \tag{4.12}$$

which gives the Jost function for the anti-symmetric channel as,

$$G_+(k) = f_+(k, 0). \tag{4.13}$$

4.1.1 Application to the Sine-Gordon Model

In section 3.1.2 we solved for the zero mode and continuum energy modes of the Sine-Gordon model by considering fluctuations around the kink solution. We can use those modes, Eq. (3.25), to write down the Jost solution

$$f_+(k, z) = \frac{e^{ikz}}{k + im}(k + im \tanh(mz)), \tag{4.14}$$

such that

$$f_+^{'}(k, z) = \frac{ike^{ikz}}{k + im}(k + im \tanh(mz)) + \frac{im^2 e^{ikz}}{k + im}(1 - \tanh^2(mz)). \tag{4.15}$$

By substituting the Jost solutions into Eq. (4.8) we obtain the Jost function for the symmetric channel,

$$\begin{aligned} F_+(k) &= \frac{1}{ik} f_+^{'}(k, 0) = \frac{k}{k + im} + \frac{m^2}{k}\frac{1}{k + im} \\ &= \frac{1}{k + im}\frac{1}{k}(k + im)(k - im) = \frac{k - im}{k}. \end{aligned} \tag{4.16}$$

Similarly we calculate the Jost function for the antisymmetric channel by substituting the Jost solution into Eq. (4.13),

$$G_+(k) = f_+(k, 0) = \frac{k}{k + im} = \left(F_+^*(k)\right)^{-1}, \tag{4.17}$$

and from the last relation we can conclude that F_+ and G_+ have identical phases. This implies equal scattering phase shifts in the two channels. Since the difference between these elements determines the reflection coefficients, the potential is reflectionless. The relations between the Jost function and the phase shift are summarized in section 2.5.2. We use this to analytically obtain the Jost function contribution to the energy integral

$$\nu(k) = \ln(F_+(k)G_+(k)) = \ln\left(\frac{k-im}{k+im}\right). \tag{4.18}$$

The Born approximation is the first term of the large k expansion, which is

$$\nu^{(1)}(k) = -\frac{2im}{k}. \tag{4.19}$$

4.1.2 Application to the ϕ^4 Kink

In Section 2.4.1 we considered scattering solutions for the ϕ^4 model, whilst listing an analytical solution in Eq. (2.38). The Jost solution for the ϕ^4 model just differs in normalization,

$$f_+(k,z) = Ne^{ikz}\left[\frac{3}{2}\tanh^2\left(\frac{mz}{2}\right) - \frac{1}{2} - \frac{2k^2}{m^2} - \frac{3ik}{m}\tanh\left(\frac{mz}{2}\right)\right]. \tag{4.20}$$

For simplicity we introduce $M = \frac{m}{2}$ and determine N from the asymptotic condition, Eq. (4.2),

$$\frac{2}{N} = 2 - \frac{k^2}{M^2} + 3i\frac{k}{M} = -\frac{1}{M^2}(k+2iM)(k+iM). \tag{4.21}$$

We can use this to solve for the Jost function in the antisymmetric channel

$$\begin{aligned} G_+(k) = f_+(k,0) &= -\frac{N}{2M^2}(M^2+k^2) \\ &= \frac{(k+iM)(k-iM)}{(k+2iM)(k+iM)} = \frac{k-iM}{k+2iM}. \end{aligned} \tag{4.22}$$

For the symmetric channel we require the derivative of the Jost solution, which reads

$$f_+^{'}(k,z) = ikf_+(k,z) + \frac{N}{2}e^{ikz}\left[6M\tanh(Mz)[1-\tanh^2(Mz)] - 3ik(1-\tanh^2(Mz))\right], \tag{4.23}$$

and when evaluated at $x = 0$ gives,

$$f_+^{'}(k,0) = ikf_+(k,0) - 3ik\frac{N}{2}. \tag{4.24}$$

We can use these results to obtain the Jost function in the symmetric channel,

$$\begin{aligned} F_+(k) = \frac{1}{ik}f_+^{'}(k,0) &= f_+(k,0) + \frac{3M^2}{(k+2iM)(k+iM)} \\ &= \frac{1}{k+2iM}\left[k - iM + \frac{3M^2}{k+iM}\right] = \frac{1}{(k+2iM)(k+iM)}(k^2+4M^2) \\ &= \frac{(k+2iM)(k-2iM)}{(k+2iM)(k+iM)} = \frac{k-2iM}{k+iM} = (G_+^*(k))^{-1}. \end{aligned} \tag{4.25}$$

As seen in the Sine-Gordon model F_+ and G_+ have identical phases and thus the potential is reflectionless. For the collection of results we replace the original substitution of $M = \frac{m}{2}$ to obtain,

$$F_+(k) = \frac{k-im}{k+i\frac{m}{2}} \qquad \text{and} \qquad G_+(k) = \frac{k-i\frac{m}{2}}{k+im}. \tag{4.26}$$

The zero mode is obtained at $F_+(im) = 0$ and the shape mode at $G_+(im/2) = 0$. Similarly to Eq. (4.18) we obtain the Jost function contribution for the ϕ^4 kink model,

$$\nu(k) = \ln(F_+(k)G_+(k)) = \ln\left(\frac{k-im}{k+i\frac{m}{2}}\frac{k-i\frac{m}{2}}{k+im}\right). \tag{4.27}$$

The Born approximation is once again obtained from the large k expansion,

$$\nu^{(1)}(k) = -\frac{3im}{k}. \tag{4.28}$$

4.2 Calculation of the VPE

After calculating the Jost functions and the Born approximations for the Sine-Gordon and ϕ^4 kink models, we are able to evaluate the VPE. Currently our calculations are done in terms of the real values k. Ultimately we want to express the VPE with respect to complex momenta.

If we refer back to Eq. (2.62), we can discuss the changes that need to be considered. We want to simplify the expression for the VPE using the analytic properties of the Jost function. In a first step we write, allowing a multi-channel scenario[1],

$$\delta(k) = \frac{1}{2i}\ln\,\det S(k) = \frac{1}{2i}\left[\ln\,\det F(-k) - \ln\,\det F(k)\right]. \tag{4.29}$$

The right hand side is obviously odd in k, so its derivative is even. Furthermore, if $F^{(1)}$ is the first term in the Born expansion of the Jost function $F(k) = \mathbb{I} + F^{(1)}(k) + ...$, we can express the VPE along the real axis as a single integral in the following way,

$$\begin{aligned}\Delta E =& \frac{1}{2}\sum_j^{b.s.}(\omega_j - m)\\ &- \frac{1}{2i}\int_0^\infty \frac{dk}{\pi}(\omega_k - m)\frac{d}{dk}\left[\ln\det F(k) - \ln\det F(-k) - \mathrm{tr}(F^{(1)}(k)) - \mathrm{tr}(F^{(1)}(-k))\right]\\ =& \frac{1}{2}\sum_j^{b.s.}(\omega_j - m) - \frac{1}{2i}\int_{-\infty}^\infty \frac{dk}{2\pi}(\omega_k - m)\frac{d}{dk}[\ln\det F(k) - \mathrm{tr}(F^{(1)}(k))].\end{aligned} \tag{4.30}$$

Since $F(k)$ is analytic in the upper half plane, we compute the integral by closing the contour accordingly. The Jost funtion has simple zeros at the (imaginary) bound state momenta, κ_j, as shown in Eq. (4.26). Hence

$$\frac{d}{dk}\ln\det F(k) = \sum_j^{b.s.}\frac{1}{k - i\kappa_j}. \tag{4.31}$$

In the contour integral this contributes $-\frac{1}{2}\sum_j^{b.s.}(\omega_j - m)$ and cancels the first sum in Eq. (4.30). Furthermore ω_k has a branch cut for $k = it$ with $t > m$. We exclude that cut from the contour integral and pick up the discontinuity ($\epsilon, \tilde{\epsilon} \to 0^+$),

$$\sqrt{(it+\epsilon)^2 + m^2} - \sqrt{(it-\epsilon)^2 + m^2} = \sqrt{t^2 - m^2}[\sqrt{-1 + i\tilde{\epsilon}} - \sqrt{-1 - i\epsilon}] = 2i\sqrt{t^2 - m^2}.$$

Finally integrating by parts yields the VPE,

$$\Delta E = \int_m^\infty \frac{dt}{2\pi}\frac{t}{\sqrt{t^2 - m^2}}[\nu(t) - \nu^{(1)}(t)], \tag{4.32}$$

[1]Different rows denote the channel wave-functions; different columns the (scattering) initial conditions, cf. Section 5.3.

with $\nu^{(1)}(t) = \mathrm{tr}(F^{(1)}(it))$.

We start by considering the Sine-Gordon Model. In oder to use this equation we need to rewrite Eqs. (4.18,4.19) for the transformation $k = it$ which yields

$$\nu(it) = \ln \frac{t-m}{t+m} \qquad \text{and} \qquad \nu^{(1)}(it) = -\frac{2m}{t}. \tag{4.33}$$

Thus the VPE equation for the Sine-Gordon model is given by

$$\Delta E = \int_m^\infty \frac{dt}{2\pi} \frac{t}{\sqrt{t^2-m^2}} \left[\ln \frac{t-m}{t+m} + \frac{2m}{t} \right] = -\frac{m}{\pi}. \tag{4.34}$$

This integral could be computed analytically. Unfortunately, in most models $\nu(it)$ is only obtained by numerical simulation. In chapter 6 we will therefore apply our numerical tools to the above integral to estimate the accuracy of these tools.

Next we consider the ϕ^4 kink model in the same way, starting with rewriting Eqs. (4.27,4.28) also in terms of the transformation of $k = it$,

$$\nu(it) = \ln \frac{(t-m)(t-\frac{m}{2})}{(t+\frac{m}{2})(t+m)} \qquad \text{and} \qquad \nu^{(1)}(it) = -\frac{3m}{t}. \tag{4.35}$$

This leads to the VPE equations for the ϕ^4 kink model

$$\Delta E = \int_m^\infty \frac{dt}{2\pi} \frac{t}{\sqrt{t^2-m^2}} \left[\ln \frac{(t-m)(t-\frac{m}{2})}{(t+\frac{m}{2})(t+m)} + \frac{3m}{t} \right] = m \left(\frac{1}{4\sqrt{3}} - \frac{3}{2\pi} \right). \tag{4.36}$$

The accuracy of this equation can be compared to the results from Eq. (3.37) and will also be discussed in chapter 6.

Chapter 5

Multi-component Model

5.1 Definitions

The multi-component model under investigation consists of two scalar fields. The first, denoted by ϕ, is a singlet. The second, denoted by χ_i, represents a triplet with internal degrees of freedom counted by $i = 1, 2, 3$.

5.2 Classical Solutions

The system, as introduced in Ref. [21], is described by the following Lagrangian,

$$\mathcal{L} = \frac{1}{2}\partial_\mu\phi\partial^\mu\phi + \frac{1}{2}\partial_\nu\chi_i\partial^\nu\chi_i - V(\phi) - \gamma W(\phi, \chi_i), \tag{5.1}$$

where the loop counting parameter λ has been excluded, since we have already established its physical implications. The respective potentials are

$$V(\phi) = (\phi^2 - 1)^2, \tag{5.2}$$

$$W(\phi, \chi_i) = (\phi^2 - \mu^2)\chi^2 + \beta(\chi^2)^2. \tag{5.3}$$

The variables γ, β and μ are constants, for which $\gamma, \beta \geq 0$ and $0 \leq \mu \leq 1$ are needed for a nonnegative field potential. Since $\chi^2 = \chi_i\chi_i$, neither χ^2 nor $W(\phi, \chi_i)$ depend on the orientation of χ_i in the internal space. The Lagrangian yields the full equations of motion

$$\phi'' - \ddot{\phi} = 4\phi(\phi^2 - 1) + 2\gamma\phi\chi^2 \tag{5.4}$$

$$\chi_i'' - \ddot{\chi}_i = 2\gamma\chi_i(\phi^2 - \mu^2) + 4\gamma\beta\chi^2\chi_i. \tag{5.5}$$

The stationary equations of motion are

$$\phi'' = 4\left(\phi^2 - 1\right)\phi + 2\gamma\phi\chi^2 \tag{5.6}$$

$$\chi_i'' = 2\gamma\left(\phi^2 - \mu^2\right)\chi + 4\beta\gamma\chi^2\chi_i. \tag{5.7}$$

For $\gamma = 0$, χ_i is a free massless field and the stationary equations are solved by the same ansatz we employed in the simple ϕ^4 model, $\phi_0 = \tanh\alpha z$ with $\alpha = \sqrt{2}$. The interaction between the fields is turned on for $\gamma \neq 0$. For this case ϕ_0 remains formally unchanged while for χ_i we take the ansatz of,

$$\chi_3 = \chi_0 = A\mathrm{sech}(\alpha z), \tag{5.8}$$

together with $\chi_{1,2} = 0$. Substitution of ϕ_0 and χ_0 into Eq. (5.6) yields $A = \sqrt{\frac{2-\alpha^2}{\gamma}}$. We get for Eq. (5.7) a linear combination of $\mathrm{sech}(\alpha z)$ and $\mathrm{sech}(\alpha z)\tanh^2(\alpha z)$. The coefficients of both terms must vanish, so we find two conditions,

$$\alpha^2 = 2\gamma\mu^2 - 4\gamma\beta A^2 \qquad \text{and} \qquad \alpha^2 = \gamma - 2\beta\gamma A^2. \tag{5.9}$$

They combine to $\alpha^2 = 2\gamma q$ with $q = 1 - \mu^2$ and $2\mu^2 - 1 = 2\beta A^2$. Furthermore, the combination of these equations also yields $-A^2 = \frac{2q-1}{2\beta}$, which restricts q such that

$$q < \frac{1}{2}. \tag{5.10}$$

Inserting the relation between A and α that we obtained from Eq. (5.6) leads to a consistency condition for the model parameters. We can phrase this condition as

$$\gamma = \frac{4\beta}{2q(2\beta - 1) + 1}. \tag{5.11}$$

Stated otherwise, we find the kink type solution in terms of hyperbolic functions only when β, γ and $\mu^2 = 1-q$ are related as in Eq. (5.11).

From the second relation in Eq. (5.9), we infer that $A^2 < \frac{1}{2\beta}$, which leads to $\gamma > \frac{4\beta}{1+4\beta q}$. In turn the first relation has real solutions only when $\mu^2 > 2\beta A^2 = \frac{2\beta}{\gamma}(1 - \gamma q)$. Together with the positivity conditions listed after Eq. (5.3), this implies $\gamma < \gamma_L = \frac{1}{q}$ as the upper limit. A set of parameters that obeys all these conditions is:

$$\mu^2 = 0.81, \qquad \gamma = \frac{75}{53} \sim 1.415, \qquad \beta = 0.3. \tag{5.12}$$

Finally the classical energy of the ϕ_0 and χ_0 field is obtained to be,

$$E_{cl} = \int_{-\infty}^{\infty} \left[\frac{1}{2}\left(\frac{d\phi}{dz}\right)^2 + \frac{1}{2}\left(\frac{d\chi}{dz}\right)^2 + (\phi^2 - 1)^2 + \gamma[(\phi^2 - \mu^2)\chi^2 + \beta\chi^4] \right] dz, \tag{5.13}$$

which, in terms of the parameters defined above, yields [21]

$$E_{cl} = \frac{4A^4\beta\gamma + 2(\alpha^2 + 2) + A^2(\alpha^2 + 2\gamma(3q - 2))}{3\alpha}. \tag{5.14}$$

5.3 Scattering Problem

We identify the asymptotic behaviour of the fields as $z \to \pm\infty$,

$$\phi_0 \approx \pm 1 + e^{-2\alpha|z|} \tag{5.15}$$

$$\chi_0 \approx 2Ae^{-\alpha|z|}. \tag{5.16}$$

This causes the behaviour at spatial infinity to be $\phi_0 = \pm 1$ for positive and negative infinity respectively and $\chi_0 = 0$. These asymptotic behaviors are essential when we identify the masses of the fluctuations η_1 and η_2 around these solutions,

$$\phi(t, z) = \phi_0(z) + \eta_1(t, z), \tag{5.17}$$

$$\chi_3(t, z) = \chi_0(z) + \eta_2(t, z). \tag{5.18}$$

Since the soliton background is static, we factorize $\eta_i(t,z) = e^{-i\omega t}\eta_i(z)$. We substitute these parameterisations into our equations of motion and expand up to the linear order, which is equivalent to expanding the Lagrangian to quadratic order and taking the first derivative with respect to the fields. This leads to

$$\eta_1^{''} + (\omega^2 - 8)\eta_1 = 12(\phi_0^2 - 1)\eta_1 + 2\gamma\chi_0^2\eta_1 + 4\gamma\phi_0\chi_0\eta_2, \tag{5.19}$$

$$\eta_2^{''} + (\omega^2 - 2\gamma q)\eta_2 = [2\gamma(\phi_0^2 - 1) + 12\gamma\beta\chi_0^2]\eta_2 + 4\gamma\chi_0\phi_0\eta_1, \tag{5.20}$$

as the equations of motion for the time-independent functions η_1 and η_2. From the asymptotic behaviors, Eqs. (5.15) and (5.16), we see that the right-hand-sides vanish for $|z| \to \infty$ while we read off the masses from the left-hand-sides as the smallest ω value that allows for solutions with spatial oscillations:

$$\eta_1 : \ m_1 = 2\sqrt{2},$$
$$\eta_2 : \ m_2 = \sqrt{2\gamma q}.$$

Since we require $\gamma < \frac{1}{q}$, we conclude that $m_2 < m_1$. The wave equations can also be rewritten in matrix form, to more clearly illustrate the potential matrix of our model,

$$\begin{bmatrix} \partial_z^2 + \left(\omega^2 - m_1^2\right) & 0 \\ 0 & \partial_z^2 + \left(\omega^2 - m_2^2\right) \end{bmatrix} \begin{bmatrix} \eta_1 \\ \eta_2 \end{bmatrix} = \begin{bmatrix} 12\left(\phi_0^2 - 1\right) + 2\gamma\chi_0^2 & 4\gamma\phi_0\chi_0. \\ 4\gamma\phi_0\chi_0 & 2\gamma\left(\phi_0^2 - 1\right) + 12\gamma\beta\chi_0^2 \end{bmatrix} \begin{bmatrix} \eta_1 \\ \eta_2 \end{bmatrix}, \tag{5.21}$$

where the 2×2 matrix on the right-hand side represents the potential matrix $V(z)$. The potential matrix is not reflection symmetric due to the off diagonal elements being anti-symmetric. However, the diagonal is symmetric under the transformation $z \to -z$. A discussion concerning this skewed parity will follow in a later section, as the construction of the corresponding decoupled wave functions requires some unconventional conditions on these wave functions at the center of the soliton. Keeping the matrix notation, we can once again re-organise the previous system of equations and we further simplify them via the relativistic dispersion relations $k_i^2 = \omega^2 - m_i^2$,

$$-\partial_z^2 \begin{bmatrix} \eta_1 \\ \eta_2 \end{bmatrix} = \left[\begin{bmatrix} k_1^2 & 0 \\ 0 & k_2^2 \end{bmatrix} - V(z) \right] \begin{bmatrix} \eta_1 \\ \eta_2 \end{bmatrix}. \tag{5.22}$$

We can construct two independent solutions $\eta_1^{(i)}$ and $\eta_2^{(i)}$ that asymptotically equal a plane wave in one channel while the other is absent. It is then efficient to combine them in a matrix field,

$$\begin{pmatrix} \eta_1^{(1)} & \eta_1^{(2)} \\ \eta_2^{(1)} & \eta_2^{(2)} \end{pmatrix} = F_k(z)h(z) = F_k(z) \begin{pmatrix} e^{ik_1 z} & 0 \\ 0 & e^{ik_2 z} \end{pmatrix}, \tag{5.23}$$

where $F(z)$ is the matrix of the reduced Jost solutions with the boundary condition $F(z) \to \mathbb{I}$ as $z \to \infty$. The $h(z)$ matrix simply contains the information on the plane waves in their separate channels. Note that $h(z)$ parametrizes the independent left-moving plane waves; the two columns correspond to the possible scattering channels. In the following we focus on the half-line $z \geq 0$ and take for granted that some symmetry transformation yields the wave function on the negative half-line. The construction in Eq. (5.23) straightforwardly yields a second order differential equation for the Jost solutions

$$F_k^{''}(z) = -2iF_k^{'}(z)K(k) + [M^2, F_k(z)] + V(z)F_k(z). \tag{5.24}$$

Here $K(k)$ is the matrix consisting of the independent momenta and M^2 is the diagonal mass matrix,

$$K(k) = \begin{pmatrix} k_1 & 0 \\ 0 & k_2 \end{pmatrix} \qquad \text{and} \qquad M^2 = \begin{pmatrix} m_1^2 & 0 \\ 0 & m_2^2 \end{pmatrix}. \tag{5.25}$$

5.4 Jost Function

There exist some restrictions to the previously mentioned Jost function properties when we consider two momenta that are not independent, as in our case where we have k_2 and $k_1(k_2)$. Since we consider $m_1 > m_2$ the wave number corresponding to the lighter fluctuation, k_2, will set the scale, whilst the heavier fluctuation's wavenumber will depend on k_2. We have established that the energy of the fluctuations is conserved and the relativistic dispersion relations imply

$$k_2^2 + m_2^2 = k_1^2 + m_1^2. \tag{5.26}$$

This leads to three conditions that the relation $k_1(k_2)$ must satisfy:

- Within the gap $k_2^2 < m_1^2 - m_2^2$, any real k_2-variable will result in an imaginary k_1 momentum with a purely positive imaginary part.

- Outside the gap $k_2^2 \geq m_1^2 - m_2^2$, any real k_2 will result in a real k_1 and $k_2 \to -k_2$ implies that $k_1 \to -k_1$ since it will ensure $F(-k_2) = F^*(k_2)$.

- If $\mathrm{Im}(k_2) \geq 0$ then $\mathrm{Im}(k_1) \geq 0$ must be true, to ensure both momenta are in the positive complex plane.

The Jost solution is a solution to our differential equation that depends on the coordinate and the momentum. It is analytical only in the upper half complex plane, thus we require $Im(k_i) \geq 0$. We have mentioned that our k_1 momentum depends on our k_2 momentum. For real k-values the dependency can be obtained by starting with Eq. (5.26) and using the conservation of energy. In Ref. [28] it has been shown that

$$k_1(k_2) = k_2\sqrt{1 - \frac{m_1^2 - m_2^2}{[k_2 + i\epsilon]^2}} \qquad \text{with.} \qquad \epsilon \to 0^+ \tag{5.27}$$

is consistent with the above conditions. Since $m_1 > m_2$ the radical will always be positive when $ik_2 = t > m_2$ and we can omit the $\epsilon-$prescription. Hence we get the simple relation for purely imaginary momenta

$$k_1 = it\sqrt{1 + \frac{m_1^2 - m_2^2}{t^2}} = i\sqrt{t^2 + m_1^2 - m_2^2} =: it_1(t). \tag{5.28}$$

As explained in section 4.2, we can then compute the momentum integral by contour integration.

5.4.1 From Real to Complex

We switch over to imaginary momenta and make the substitution of $k_2 = it$, to cancel our bound states in our calculation for the VPE. Using the Jost function turns our VPE calculation into a single integral along the branch cut $t \geq m_2$ with both of the different mass scales included. The additional singularity originating from the $\epsilon-$prescription has no effect, because $t = -i\epsilon$ is in the lower half plane. This procedure is superior to solving the problem for real momentum since on the real axis three different momentum regimes must be considered.

When applying the continuation to the wave equation, Eq. (5.18) becomes,

$$F_k^{''}(z) = 2F_k^{'}(z)D(t) + [M^2, F_k(z)] + V(z)F_k(z), \tag{5.29}$$

where $D(t)$ contains the imaginary momenta for both channels

$$D(t) = \begin{pmatrix} t_1 & 0 \\ 0 & t \end{pmatrix} \tag{5.30}$$

so that Eq. (5.29) is a real variable differential equation. To understand the physics behind this equation we consider various solutions to the scattering problem, namely the Jost solution, the regular solution and the physical scattering solution. Each of these solutions has its own boundary condition. Previously we have seen the physical solution, ϕ which is regular at $z = 0$. Similarly, the physical scattering solution in the antisymmetric channel is also regular and is of the form $\sin(kz+\delta)$ at spatial infinity. These solutions are not linearly independent. The boundary conditions to the physical solution does not depend on the parameters in our differential equation, thus the solutions are analytic functions of these parameters. For the Jost solution to the wave equation the situation is more complicated since the boundary condition contains k,

$$f_{\pm}(k, z) \to e^{\pm ikz}, \tag{5.31}$$

as $z \to \infty$. Typically the matrix with the Jost functions is extracted from the Jost solution and its derivative at $z = 0$, cf. chapter 4. This generalizes to the matrix case, though the antisymmetry of the off-diagonal elements in $V(z)$ requires a more sophisticated definition of parity.

Analyticity of the Jost solution can be established by writing a perturbation expansion for a specific potential matrix in the case of the upper half of the complex plane. This allows us to perform the analytic continuation if needed. When considering all these solutions together, since they depend on each other, we can consider a regular solution as mentioned in Eq.(4.4), which is symmetric under a $k \to -k$ transformation. This solution not only contains the scattering solutions but also the bound states since we defined $k \in \mathbb{C}$ and consists of exponential increasing and decreasing functions. At the bound state momentum we need,

$$\varphi(k, z) \to e^{-\kappa z}, \qquad \text{for} \qquad z \to \infty, \tag{5.32}$$

with $\kappa > 0$. For $k = i\kappa$, Eq. (4.2) implies $f_+(k, z) \to e^{-\kappa z}$ and $f_-(k, z) \to e^{\kappa z}$. Hence the required asymptotic behavior that bound state wave functions approach zero at spatial infinity, emerge from Eq. (4.4) only when $F_+(i\kappa) = 0$. Alternatively stated, $F_+(i\kappa) = 0$ if $k = i\kappa$ is a bound state wave number, which are located on the imaginary axis. These are the only zeros of the Jost function on the upper half plane.

There are various reasons why we calculate the VPE on the imaginary instead of the real axis. The advantages are:

- The differential equation (though very similar) becomes real for imaginary momenta.
- During the calculation of the VPE, we do not need to explicitly search for the bound states as they are included in the residue of the derivative of the logarithm of the Jost function.
- When numerically extracting the phase shift we obtained for real momenta, we noticed a jump between $-\pi$ and π, which is difficult to identify. On the imaginary axis the same information is portrayed by a smooth real function namely $\ln F(k)$.

- For real values, when considering the energy gap and the scattering solutions, we note that not all channels are open. With increasing energy they open up and threshold cusps appear that are difficult to handle numerically.

These reasons are already sufficient motivation for completing our calculation in the complex plane.

Furthermore, we need to define the Jost functions for the symmetric and antisymmetric channel to aid the calculations associated with parity. This is done by considering the scattering solutions, which are expressed as linear combinations of F_k, which possesses the property $F_k^* = F_{-k}$ for real momenta. The symmetric and anti-symmetric wave functions decouple due to the symmetry of the potential $V(-z) = V(z)$. Consider the symmetric channel wave function

$$\psi_S = F_k^*(z)e^{-iKz} + F_k(z)e^{iKz}S_S, \tag{5.33}$$

where S_S denotes the symmetric $S-$matrix and K is defined in Eq. (5.25). Note that the condition, Eq. (5.27), is such that this parametrization is also applicable for $m_1 < \omega < m_2$ with imaginary k_1. For the symmetric channel, we consider the boundary condition associated with the derivative of the wave function, $\psi_S^{'}(0) = 0$, which yields

$$(F_k(z)^{'*} - iF_k^*(z)K) + (F_k^{'}(z) + iF_k(z)K)S_S = 0. \tag{5.34}$$

The sum of the eigenphase shifts, defined by the determinant of the scattering matrix, is therefore expressed as

$$\det[S_S] = \det[F_S^{-1}(k)F_S(-k)], \tag{5.35}$$

where

$$F_S(k) = \lim_{z\to 0}[F_k(z) - iF_k^{'}(z)K^{-1}]. \tag{5.36}$$

Similarly the wave fucntion for the symmetric channel is

$$\psi_A = F_k^*(z)e^{-iKz} + F_k(z)e^{iKz}S_A. \tag{5.37}$$

When evaluating for the boundary conditions $\psi_A(0) = 0$, we find the relation $F_k^*(z) + F_k(z)S_A = 0$ such that the eigenphase shift is defined by

$$\det[S_A] = \det[F_A^{-1}(k)F_A(-k)], \tag{5.38}$$

so that the Jost function in the anti-symmetric channel is

$$F_A(k) = \lim_{z\to 0} F_k(z). \tag{5.39}$$

The change in the density of the scattering states is given by the derivative of the total phase shifts [28]

$$\delta_i = \frac{1}{2i}[\ln\det F_i(-k) - \ln\det F_i(k)] \tag{5.40}$$

where $i = S, A$. Finally the symmetric and anti-symmetric Jost functions are combined in the full Jost function for the multi-component model as the logarithm of the determinant for the analytic continuation $k = it$,

$$\nu^{(1)}(t) = \ln\det[F_S(it)F_A(it)]. \tag{5.41}$$

5.4.2 Jost Function for Skewed Parity

We want to solve the scattering problem defined by Eq. (5.21) with antisymmetric off-diagonal potential matrix elements. The discussion, so far, is based on decoupled channels for reflection symmetric and anti-symmetric wave-functions. This decoupling only occurs when the potential matrix is symmetric; i.e. $V(-z) = V(z)$. Unfortunately this is not a property of the potential matrix in Eq. (5.21). Rather, and similar to the Dirac theory, the potential matrix is invariant under skewed parity,

$$V(-z) = \begin{pmatrix} 1 & 0 \\ 0 & -1 \end{pmatrix} V(z) \begin{pmatrix} 1 & 0 \\ 0 & -1 \end{pmatrix}. \tag{5.42}$$

We can introduce a parity operator like in the Dirac theory with eigenvalues $\lambda_p = \pm 1$ such that,

$$\hat{P} = \begin{pmatrix} 1 & 0 \\ 0 & -1 \end{pmatrix} \otimes [z \to -z], \tag{5.43}$$

We now have two parity channels, one associated with $\lambda_p = 1$ and the other with $\lambda_p = -1$. We define the two projector matrices,

$$P_+ = \begin{pmatrix} 1 & 0 \\ 0 & 0 \end{pmatrix} \qquad P_- = \begin{pmatrix} 0 & 0 \\ 0 & 1 \end{pmatrix}, \tag{5.44}$$

to assist in expressing the important quantities with respect to the two channels. When applied to the $\lambda_p = +1$ wave function,

$$\hat{P} \begin{pmatrix} \eta_1(z) \\ \eta_2(z) \end{pmatrix} = \begin{pmatrix} \eta_1(z) \\ \eta_2(z) \end{pmatrix} = \begin{pmatrix} \eta_1(-z) \\ -\eta_2(-z) \end{pmatrix}, \tag{5.45}$$

we find that respectively we have $P_+\eta_+$ is symmetric under $z \to -z$ and $P_-\eta_+$ is anti-symmetric. This implies that

$$P_+\eta_+^{'}(0) = 0 = P_-\eta_+(0). \tag{5.46}$$

We construct the scattering wave-function with positive skewed parity as

$$\eta_+ = F_{-k}(z)e^{-iKz}D(-k) + F_k(z)e^{iKz}D(k)S_+, \tag{5.47}$$

where the diagonal matrix $D(k)$ will be determined later from the condition that when the potential is turned off, $V(z) = 0$, the Jost matrix becomes the identity. To compute the scattering matrix S_+, we apply (5.46) and identify the limit $z \to 0$ from Eqs. (5.36) and (5.39)

$$P_+F_S(-k)iKD(-k) - P_+F_S(k)iKD(k)S_+ = 0, \tag{5.48}$$

$$P_-F_A(-k)D(-k) + P_-F_A(k)D(k)S_+ = 0. \tag{5.49}$$

In order to establish Jost functions $F_\pm$ that later will be subject to analytic continuation, we subtract the two previously mentioned equations from one another, disregarding the different units, since we will only need the determinant of $F_\pm$ (cf. Wronskian). We start by defining F_+ as

$$F_+(k) = [P_+F_S(k)iK + P_-F_A(k)]D(k). \tag{5.50}$$

This implies that the scattering matrix is given by

$$S_+ = -F_+^{-1}(k)F_+(-k) \tag{5.51}$$

The overall negative sign can be ignored as we are interested in the determinant of S_+ and the determinant of the negative identity matrix yields positive one. We construct the matrix $D(k)$ by solving Eq. (5.50) for $V(z) = 0$, which implies $F_S = F_A$ and requires that also $F_+ = \mathbb{I}$ in this case. This gives

$$D(k) = \begin{pmatrix} -\frac{i}{k_1} & 0 \\ 0 & 1 \end{pmatrix}. \tag{5.52}$$

Substituting this matrix back into Eq. (5.50) leads to the complete Jost function for the symmetric channel

$$F_+(k) = P_+ F_S(k) \begin{pmatrix} 1 & 0 \\ 0 & ik_2 \end{pmatrix} + P_- F_A(k) \begin{pmatrix} -\frac{i}{k_1} & 0 \\ 0 & 1 \end{pmatrix}. \tag{5.53}$$

Similarly, the Jost function of the anti-symmetric channel is given as

$$F_-(k) = P_- F_S(k) \begin{pmatrix} ik_1 & 0 \\ 0 & 1 \end{pmatrix} + P_+ F_A(k) \begin{pmatrix} 1 & 0 \\ 0 & -\frac{i}{k_2} \end{pmatrix}. \tag{5.54}$$

By combining Eqs. (5.53,5.54) we can compactly write the full Jost matrix as [29],

$$F_\pm(k) = [P_\pm F_S(k) D_\mp(k) + P_\mp F_A(k) D_\pm^{-1}(k)]. \tag{5.55}$$

For complex momenta $t = -ik_2$ and $t_1 = \sqrt{t^2 + m_1^2 - m_2^2} = ik$, $D_\pm(k)$ is given by,

$$D_+(ik) = \begin{pmatrix} -t_1 & 0 \\ 0 & 1 \end{pmatrix} \qquad D_-(ik) = \begin{pmatrix} 1 & 0 \\ 0 & -t \end{pmatrix}. \tag{5.56}$$

From the full definition of the Jost matrices we then obtain the Jost function for the imaginary momenta as,

$$\nu(t) = \ln(\det[F_+(it) F_-(it)]). \tag{5.57}$$

Which is essential for the VPE calculation. We also note that

$$F_S(it) = \lim_{z \to 0} [F_{it}(z) - F_{it}^{'} D^{-1}(t)], \tag{5.58}$$

with $D(t)$ given by Eq. (5.30)

5.5 VPE

The first topic to discuss is the potential matrix used up until this point. The potential matrix given in Eq. (5.21) is the potential for the ϕ_0 and χ^3 components. The full potential matrix for the scalar field and triplet is actually a 4×4 matrix denoted by,

$$\overline{V}(z) = \begin{bmatrix} 2(6\phi_0^2 - 6 + \gamma\chi_0^2) & 0 & 0 & 4\gamma\phi_0\chi_0 \\ 0 & 2\gamma(\phi_0^2 - 1) + 4\beta\gamma\chi_0^2 & 0 & 0 \\ 0 & 0 & 2\gamma(\phi_0^2 - 1) + 4\beta\gamma\chi_0^2 & 0 \\ 4\gamma\phi_0\chi_0 & 0 & 0 & 2\gamma(\phi_0^2 - 1) + 12\beta\gamma\chi_0^2 \end{bmatrix}. \tag{5.59}$$

This matrix decouples into two channels, of which the first consist of the previously mentioned ϕ_0 and χ^3 skewed parity system and the second channel is the identical χ^1 and χ^2 system, which is merely a single channel problem that can be treated like two copies of the kink problem.

We start the discussion of the multi-components' VPE calculation by considering the decoupled system containing ϕ_0 and χ^3, since the single channel problem is much easier. We adopt the construction from section 5.4.2 for

$$V(z) = \begin{pmatrix} \overline{V}_{11} & \overline{V}_{14} \\ \overline{V}_{41} & \overline{V}_{44} \end{pmatrix} \tag{5.60}$$

to compute $\nu(t)$ from Eq. (5.57) and obtain the VPE

$$\Delta E_2 = \int_{m_2}^{\infty} \frac{dt}{2\pi} \frac{t}{\sqrt{t^2 - m_2^2}} [\nu(t) - \nu^{(1)}(t)]. \tag{5.61}$$

The Born approximation is given by

$$\nu^{(1)}(t) = \delta^{(1)}(it) = \int_0^{\infty} dz \left[\frac{\overline{V}_{11}(z)}{\sqrt{t^2 + m_1^2 - m_2^2}} + \frac{\overline{V}_{44}(z)}{t} \right]. \tag{5.62}$$

For the full VPE we need to add a similar contribution from the single channel problems for χ^1 and χ^2. Since the potential for both these cases are identical we simply calculate one of them and add the contribution twice. The calculation is very simple in comparison to the previous channel due to the solution of the differential equation Eq. (5.29) being a single Jost function $F_k^{(\text{single})}(z)$ for the reflection symmetric potential

$$V_{\text{single}}(z) = \overline{V}_{22} = \overline{V}_{33} = 2\gamma(\phi_0^2 - \mu^2) + 4\beta\gamma\chi_0^2, \tag{5.63}$$

where the subscript 'single' distinguishes the single channel-contribution. Since the single channel functions do not contain the skewed parity we merely require the symmetric and antisymmetric Jost functions

$$F_+^{\text{single}}(k) = F_k^{\text{single}}(z) \tag{5.64}$$

$$F_-^{\text{single}}(z) = F_k^{\text{single}}(z) - \frac{i}{k} F_k'^{\text{single}}(z). \tag{5.65}$$

Thus the Jost function simplifies to,

$$\nu_{\text{single}}(t) = \ln[F_+^{\text{single}}(it) F_-^{\text{single}}(it)], \tag{5.66}$$

and similarly the first Born approximation to,

$$\nu_{\text{single}}^{(1)}(t) = \int_0^{\infty} dz \frac{V_{\text{single}}(z)}{t}. \tag{5.67}$$

The VPE corresponding to the single channel is

$$\Delta E_1 = \int_{m_2}^{\infty} \frac{dt}{2\pi} \frac{t}{\sqrt{t^2 - m_2^2}} [\nu_{\text{single}}(t) - \nu_{\text{single}}^{(1)}(t)], \tag{5.68}$$

since the fluctuation modes χ_1 and χ_2 have mass m_2. Finally the complete VPE for the multi-channel model in the no-tadpole renormalization scheme becomes

$$\Delta E = \Delta E_2 + 2\Delta E_1. \tag{5.69}$$

The single-channel formalism also applies to the kink soliton with $\phi = \tanh(\sqrt{2}z)$ and $\chi = 0$. In that case we have a diagonal 4×4 potential matrix with $V_{11} = 12\text{sech}^2(\sqrt{2}z)$ and $V_{22} = V_{33} = V_{44} = 2\gamma\text{sech}^2(\sqrt{2}z)$. The potential V_{11} is of Poschl-Teller form with $n = 2$ and $m = m_1 = \sqrt{8}$. As shown in Eq. (4.36) its VPE is $\sqrt{2}\left(\frac{1}{2\sqrt{3}} - \frac{3}{\pi}\right) \approx -0.9422$. To this we add three times the VPE for V_{22} that is computed numerically as in Eq. (5.68) so that

$$\Delta E[\chi = 0] = \sqrt{2}\left(\frac{1}{2\sqrt{3}} - \frac{3}{\pi}\right) + 3\Delta E_1[\chi = 0]. \tag{5.70}$$

Chapter 6

Numerical Results

In this chapter we discuss our numerical findings. We first explore the accuracy of the numerical simulations by comparison with various analytically known results.

6.1 Numerical Tools

A number of numerical tools are used to either optimize the running time of the code or to effectively calculate different sections of the process. The main objective is to solve Eq. (5.29) subject to the boundary condition $F_{it}(z) \to \mathbb{I}$ as $z \to \infty$ (from now on we omit the subscript: $F(z) = F_{it}(z)$). For this purpose we utilize a fourth order Runge-Kutta method supplemented by an adaptive step size algorithm. More details on these tools are provided in appendices.

6.2 Born Series

We have seen that we can solve our differential equation by integrating from spatial infinity to zero, obtaining the matrix $F(z)$. The logarithm of the Jost function can symbolically be written as

$$\nu = \lim_{z \to 0} \ln(\det(F(z))). \tag{6.1}$$

As discussed in previous sections, we want to subtract the Born approximation from the Jost function. To identify the Born approximation of the Jost function we expand

$$\nu = \lambda\nu_1 + \lambda^2\nu_2 + \dots , \tag{6.2}$$

where λ is simply used for counting orders, similar to time independent perturbation theory in quantum mechanics. We then include this counting parameter in the differential equation as the strength of the potential,

$$F'' = 2F'D + [M^2, F] + \lambda VF. \tag{6.3}$$

Next we Taylor expand the Jost solution F as

$$F = \mathbb{I} + \lambda F_1 + \lambda^2 F_1 + \dots \tag{6.4}$$

and solve Eq. (6.3) order by order in λ. The expansion, Eq. (6.4) implies the boundary condition is $\lim_{z\to\infty} F_i(z) = 0$. At linear order we get,

$$\lambda F_1^{''} = 2\lambda F_1^{'} D + \lambda[M^2, F_1] + \lambda V, \tag{6.5}$$

which implies,

$$F_1^{''} = 2F_1^{'} D + [M^2, F_1] + V. \tag{6.6}$$

This leads to ν_1 being the linear order of,

$$\ln\det(\mathbb{I} + \lambda F_1) = \mathrm{tr}\ln(\mathbb{I} + \lambda F_1) \sim \lambda \mathrm{tr}(F_1), \tag{6.7}$$

at $z = 0$; i.e. $\nu_1 = \lim_{z\to 0}\mathrm{tr}(F_1(z))$. Alternatively, as shown in Eq. (5.62) ν_1 can be obtained from the integral of the potential.

6.3 Results for VPE

6.3.1 Verifying Accuracy

As stated in the beginning of this chapter, we start by comparing numerical results to known results from the literature. Since we have verified the analytical equations for the VPE for the Sine-Gordon model and the ϕ^4-Kink, we can easily compare them to our numerical results and estimate the accuracy by referring to the relative error. The table 6.1 displays the results of the simmulation.

Table 6.1: Sine-Gordon Model

	A: E_1	N: E_2	N: E_3	Er_1	Er_2
$m = 2\sqrt{2}$	-0.900316	-0.900316	-0.900316	8.6065×10^{-7}	1.9861×10^{-7}
$m = 1$	-0.31831	-0.31831	-0.31831	1.0299×10^{-5}	1.0767×10^{-5}
$m = 2$	-0.63662	-0.63662	-0.63662	3.1833×10^{-6}	3.7451×10^{-6}

In the first column the specific mass used for each result can be found. Listed in the second column are the analytical results for the Sine-Gordon model from section 3.1.3 ($VPE = -\frac{m}{\pi}$) to which the numerical results are compared. Column two has the numerical evaluation of the integral in Eq. (4.34), while column three contains the results from numerical solution to the differential equation for the Jost function substituted into the integral of Eq (4.34). The integrable square root singularity must be treated carefully. First we introduce t_{min} slightly larger than m and t_{max} large enough so that $\nu(t) - \nu^{(1)}(t) = Kt^{-3}$ for $t > t_{max}$. We fit the constant K to data from the differential equation and integrate analytically. Similarly we analytically integrate a logarithmic fit to $\nu(t) - \nu^{(1)}(t) \sim \overline{K}\ln(t - m)$ over the interval $[m, t_{min}]$ (here m denotes the smallest of the masses). More details on this procedure are provided in appendix C. The major part of the integral, from t_{min} to t_{max}, is formulated as an ordinary differential equation

$$\frac{d(\Delta E)}{dt} = \frac{1}{2\pi}\frac{t}{\sqrt{t^2 - m^2}}[\nu(t) - \nu^{(1)}(t)], \tag{6.8}$$

and integrated using an adaptive step size algorithm. The sum of the three pieces is not sensitive to the choices of t_{min} and t_{max} as long as the former is not taken too large and the latter too small. We adopt this procedure for all numerical momentum integrals.

Each numerical result is compared to the analytical result by evaluating the relative error,

$$\text{error} = \frac{|\mathrm{E_1} - \mathrm{E_i}|}{\mathrm{E_1}},$$

where $i = 2, 3$ for each result respectively. The final two columns contain the error values, where Er_1 corresponds to the difference between E_1 and E_2 while Er_2 is the difference between E_1 and E_3. All errors are relatively small since the largest error is of the order 10^{-5}, thus proving a high level of accuracy for the simulation so far.

It is worth redoing the accuracy test for the ϕ^4-Kink model since the analog numerical simulation was used. The results are displayed in table 6.2 similarly to table 6.1. Once again a high level of accuracy is

Table 6.2: ϕ^4 Model

	A: E_1	N: E_2	N: E_3	Er_1	Er_2
$m = 2\sqrt{2}$	-0.942226	-0.942227	-0.942226	1.2651×10^{-6}	5.0607×10^{-7}
$m = 1$	-0.333127	-0.333124	-0.333124	8.0515×10^{-6}	8.4989×10^{-6}
$m = 2$	-0.666255	-0.666253	-0.66625	2.8627×10^{-6}	3.5784×10^{-6}

confirmed, since largest relative error is about 10^{-6}.

Furthermore we perform a threshold test. We choose a potential matrix whose diagonal elements are sine-Gordon problems with different masses (m_1, m_2) while the off diagonal elements are zero. Then the VPE can be compared to the analytical results given by Eq. (4.34) for two masses, which simply becomes the sum. Another high level of accuracy is assured since the relative error is once again very small. Results are listed in table 6.3.

Table 6.3: Threshold Test

Mass 1	Mass 2	A: VPE	N: VPE	Error
$m_1 = 1.5$	$m_2 = 0.7$	-0.7003	-0.7001	2.53×10^{-4}
$m_1 = 2$	$m_2 = 1$	-0.9549	-0.9549	1.69×10^{-5}
$m_1 = 2.5$	$m_2 = 1$	-1.0186	-1.0200	1.27×10^{-3}
$m_1 = 2.5$	$m_2 = 1.2$	-1.1777	-1.1780	2.50×10^{-4}
$m_1 = 2.8$	$m_2 = 1.3$	-1.3051	-1.3052	8.93×10^{-5}

The reason for the lower accuracy is due to the two different mass scales which causes two different ranges in the potential matrix (5.60). This is numerically difficult to address, because at moderate and large z we have to compare tiny numbers with extremely tiny numbers.

6.3.2 Verifying Skewed Parity

The results up to this point confirm the accuracy of the single channel problems. We still need to consider the results obtained by implementing the skewed parity formalism developed in section 5.4.2. A model with two fields ϕ and χ and the Lagrangian

$$\mathcal{L} = \frac{1}{2}(\partial_\mu \phi)^2 + \frac{1}{2}(\partial_\mu \chi)^2 - \frac{1}{2}[\phi^2 + \chi^2 - 1]^2 - 2\chi^2\phi^2 \tag{6.9}$$

is equivalent to two copies of kinks with $\varphi_{1,2} = \frac{1}{\sqrt{2}}(\phi \pm \chi)$ and

$$\mathcal{L} = \frac{1}{2}(\partial_\mu \varphi_1)^2 + \frac{1}{2}(\partial_\mu \varphi_2)^2 - (\varphi_1^2 - \frac{1}{2})^2 - (\varphi_2^2 - \frac{1}{2})^2. \tag{6.10}$$

Setting $\lambda = 4$ and $m = 2$ in Eqs. (3.24) and (4.36) immediately gives $\Delta E = \left(\frac{1}{\sqrt{3}} - \frac{6}{\pi}\right)$. On the other hand we can place the φ_1 and φ_2 kinks a distance $2z_0$ apart. Then

$$\phi(z) = \frac{\sinh(2z)}{\cosh(2z_0) + \cosh(2z)} \qquad \text{and} \qquad \chi(z) = \frac{\sqrt{\cosh^2(2z_0) - 1}}{\cosh(2z_0) + \cosh(2z)}, \tag{6.11}$$

yield the potential matrix

$$V(z) = 6 \begin{pmatrix} \phi^2 + \chi^2 - 1 & 2\chi\phi \\ 2\chi\phi & \phi^2 + \chi^2 - 1 \end{pmatrix}, \tag{6.12}$$

with skewed parity symmetry.

We have subjected the potential in Eq. (6.12) to the skewed parity formalism in the numerical simulation for several values of z_0. Compared to the double kink VPE, the relative error was always less than 10^{-5}.

6.3.3 Instability

Gani et al. suggested that for $\gamma < \gamma_2 = \frac{q}{(1-q)^2}$ the soliton with $\chi_3 \neq 0$ would not be stable, rather $\phi = \tanh(\sqrt{2}z)$ and $\chi_3 = 0$ would be preferred. We first test this by comparing the classical energy of the case where $\chi_3 = 0$ obtained from Eq. (5.13) to various classical energies from Eq. (5.14). The results are displayed in table 6.4. For $\gamma > \gamma_2$ the classical energy of the $\chi = 0$ is the greater one. For $\gamma < \gamma_2$ the order is reversed. This confirms the Gani et al. suggestion.

Table 6.4: Classical energy for the soliton of Eq(5.8). The classical energy of the $\chi_3 = 0$ soliton is $\frac{4\sqrt{2}}{3} \sim 1.8856$, for all model parameters.

γ	$q = 0.15$	$q = 0.25$	$q = 0.35$	$q = 0.45$
γ_2	0.2076	0.4444	0.8284	1.4876
$\gamma = 0.2$	1.9106	2.4244	2.8187	3.1396
$\gamma = 0.5$	1.4717	1.8333	2.0903	2.2808
$\gamma = 1.2$	1.3467	1.6353	1.8127	1.9168
$\gamma = 1.7$	1.3695	1.6451	1.8010	1.8772
$\gamma = 2.1$	1.4035	1.6753	1.8206	1.8810

In order for a solution to be stable we require $\omega_i^2 \geq 0$ for all bound states. Gani et al. reached their conclusion by only constructing the bound states of the $\chi_3 = 0$ soliton. They then identified a negative ω^2 candidate for $\gamma > \gamma_2$. Certainly this signals the instability of the solution, but it makes no statement for the other, $\chi_3 \neq 0$, solution. Even though we do not construct the bound state wave-functions we have tools at hand to not only reproduce the Gani et al. bound state energies but also to explore the other soliton for $\gamma > \gamma_2$. The bound states yield zeros for the Jost functions for imaginary momenta t_i, where $\omega_i^2 = m_2^2 - t_i^2$. Hence we only have to find the zeros of the Jost function on the imaginary momentum axis which is precisely what we compute. First, however, let us make a technical remark. Since the VPE is calculated using the logarithm of the Jost function, whenever the Jost function is negative the VPE cannot be obtained. The deeper reason is that standard canonical quantization fails for imaginary frequencies. The lower bound of the integral calculation is $t = m_2$, so we require $\det(F(t)) > 0$ for all $t > m_2$ to calculate the VPE. For each stable solution we see that this is the case.

Figure (6.1) illustrates the case where $\gamma < \gamma_2$, for which the $\chi_3 = 0$ case is stable. There are no off-diagonal elements in $\overline{V}$ for that case and the full Jost function is just the product of the single-channel Jost

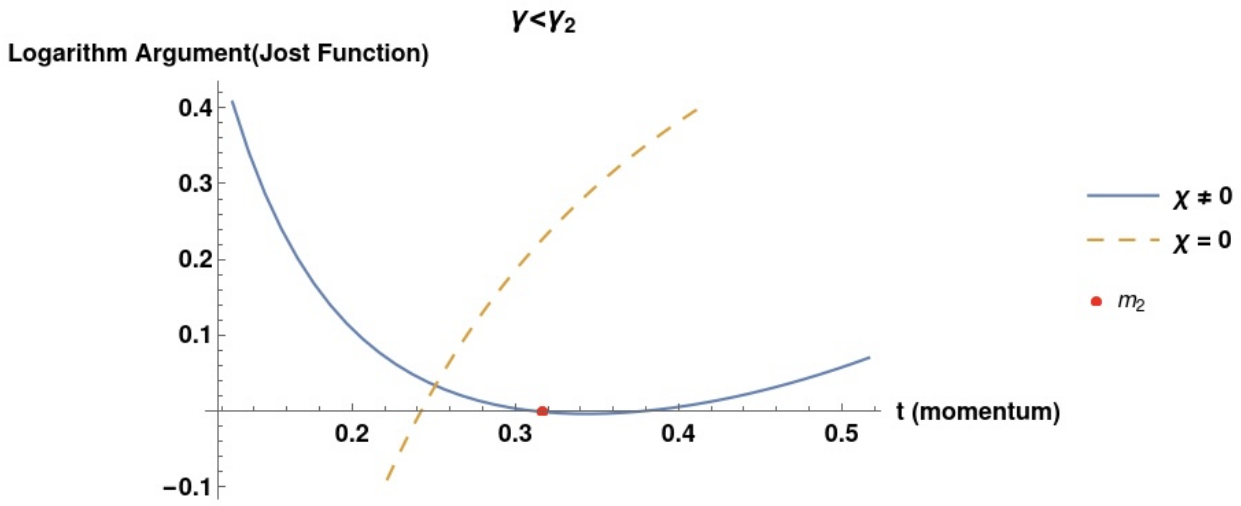

Figure 6.1: Jost functions from the potential matrix $V(z)$, Eq (6.12). The parameters are $\gamma = 0.2, q = 0.25$ implying $\gamma_2 \sim 0.44$ and $m_2 = 0.316$. The two lines correspond to the distinct solutions to the stationary field equations (5.6) and (5.7).

functions of $\overline{V}_{11}, \overline{V}_{22}, \overline{V}_{33}$ and $\overline{V}_{44}$. Since the latter three are identical we only need to find the zeros of the product of the Jost functions for $\overline{V}_{11}$ and $\overline{V}_{44}$. The former is a Poschl-Teller potential with $n = 2$ and mass parameter $m_1 = \sqrt{8}$. It also leads to the translational zero mode and hence a zero crossing of the Jost function at $t_1 = m_1$, which corresponds to $t = m_2$. For the $\chi_3 = 0$ solution $\overline{V}_{44}$ induces a second zero crossing below m_2. This verifies the Gani et al. calculation, and this solution is (locally) stable. In addition, we can identify the bound state energies for the $\chi_3 \neq 0$ soliton as well. As expected, there is a second zero crossing at $t > m_2$ corresponding to the instability of this configuration. Figure (6.2) shows that the order of zero crossings is reversed for the $\chi_3 \neq 0$ configuration when $\gamma > \gamma_2$, so that the second crossing is below m_2. It is thus stable. On the other hand, the $\chi_3 = 0$ now has a zero crossing above m_2 and is unstable.

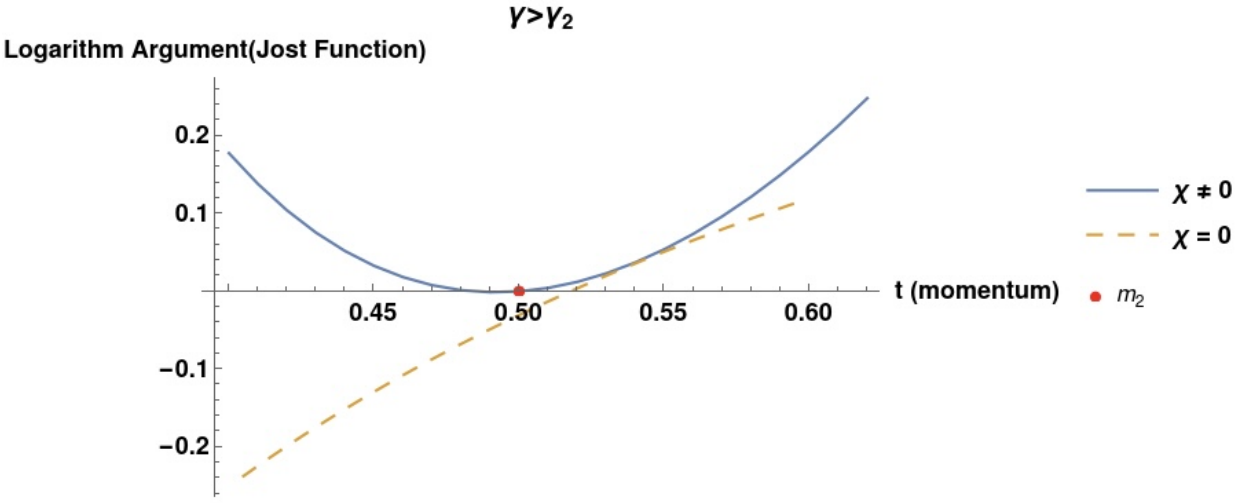

Figure 6.2: Same as Figure 6.1 for $\gamma = 0.5$, implying $m_2 = 0.5$; q and thus γ_2 as above.

Actually there is another zero mode of the $\chi_3 \neq 0$ configuration, independent of whether $\gamma > \gamma_2$ or $\gamma < \gamma_2$. The model has an $SO(3)$ symmetry amongst the χ_i. By choosing $\chi_3 \neq 0$ but $\chi_1 = \chi_2 = 0$, we break this symmetry spontaneously. A Goldstone mode must exist in that case, which we see in figures (6.3) and (6.4), with a zero crossing at m_2. Since the $\chi_i = 0$ soliton does not break this $SO(3)$ symmetry,

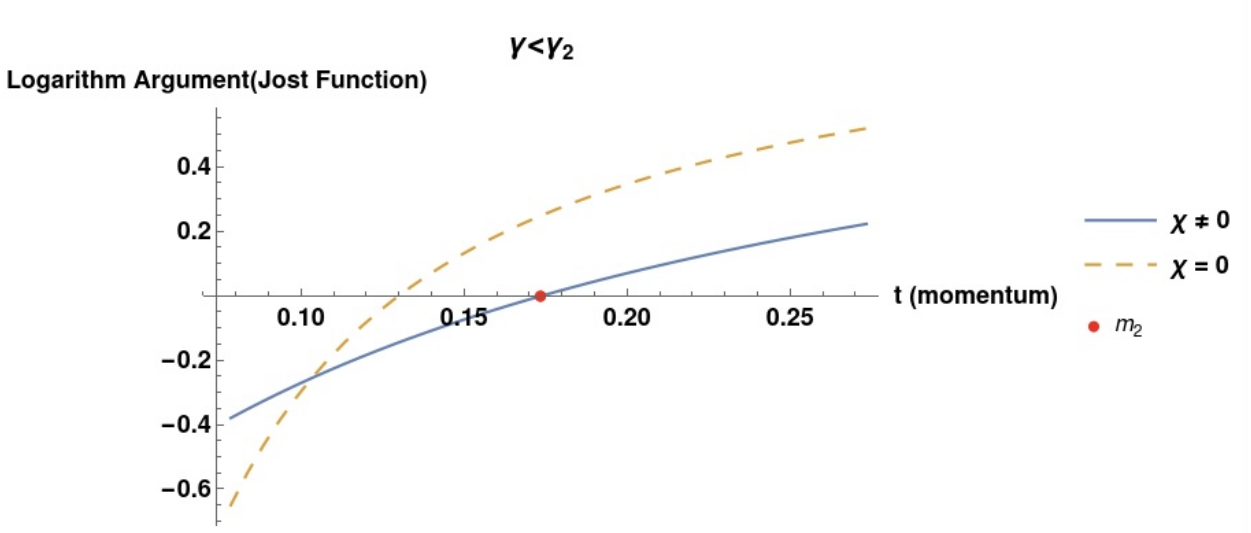

Figure 6.3: Jost functions from $\overline{V}_{22}$ for $q = 0.15$, $\gamma = 0.45$ and $\gamma_2 = 0.21$

that configuration does not have such a zero crossing. We can see this analytically because the $\chi_3 \neq 0$ configuration has $\overline{V}_{22} = -2\frac{m_2^2}{\cosh^2(m_2 z)}$, which is a Poschl-Teller potential with $n = 1$. It has a zero mode bound state with wave function $\text{sech}(m_2 z)$. This is exactly what we get for χ_2 or (χ_1) when we apply an infinitesimal $SO(3)$ transformation on $\vec{\chi} = \begin{pmatrix} 0 \\ 0 \\ A\text{sech}(m_2 z) \end{pmatrix}$.

The analog to figure (6.3) is displayed in figure (6.4) for the case where $\gamma < \gamma_2$. It is clear that figure

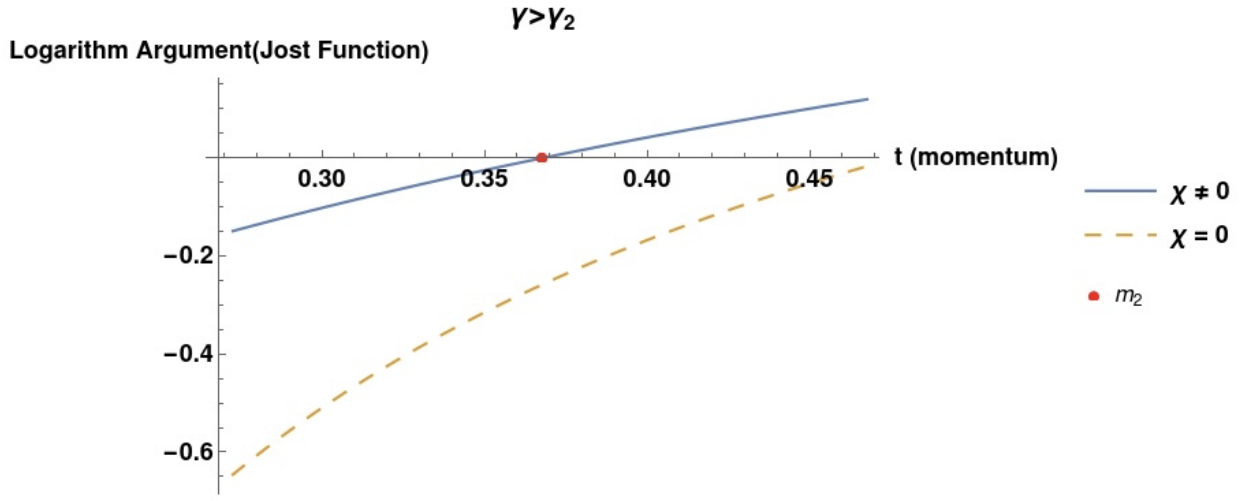

Figure 6.4: Jost functions from $\overline{V}_{22}$ for $q = 0.15$, $\gamma = 0.10$ and $\gamma_2 = 0.21$

(6.3) confirms that the $\chi_3 = 0$ soliton is stable for $\gamma < \gamma_2$ since a zero crossing below m_2 is observed and figure (6.4) confirms its instability for $\gamma > \gamma_2$ due to the zero crossing above m_2.

6.3.4 Final results for the VPE

In this section we present our main results for the VPE of the soliton in the multi-component model. The results are displayed as dimensionless numbers. Nevertheless they cannot be straightforwardly combined with the dimensionless classical energy computed above, because of being the undetermined relative loop-counting parameter discussed in Eq. (2.22). For simplicity we have omitted that factor in tables 6.4 and beyond.

We discuss the VPE results for both the $\chi_3 = 0$ and $\chi_3 \neq 0$ solitons. The results for the $\chi_3 = 0$ soliton as computed from Eq (5.70) are tabulated in table 6.5 and illustrated in figure (6.5).

Table 6.5: $\chi = 0$ VPE results (missing entries relate to parameters for which this soliton is not stable)

	$q = 0.15$	$q = 0.25$	$q = 0.35$	$q = 0.45$
$\gamma_2 \rightarrow$	0.2076	0.4444	0.8284	1.4876
$\gamma = 0.05$	-1.7155	-1.7103	-1.7080	-1.7067
$\gamma = 0.10$	-1.7469	-1.7282	-1.7209	-1.7168
$\gamma = 0.15$	-1.7987	-1.7520	-1.7370	-1.7291
$\gamma = 0.20$	-1.7987	-1.7819	-1.7559	-1.7431
$\gamma = 0.25$		-1.8185	-1.7773	-1.7585
$\gamma = 0.30$		-1.8637	-1.8014	-1.7752
$\gamma = 0.35$		-1.9211	-1.8279	-1.7932
$\gamma = 0.40$		-2.0010	-1.8572	-1.8122
$\gamma = 0.80$			-2.2942	-2.0053
$\gamma = 1.45$				-2.6329

As previously discussed, this soliton is stable for $\gamma < \gamma_2$. The VPE decreases non-linearly but monotonously as γ is increased towards γ_2 for each specific q parameter. There is also a clear increase of the VPE when increasing q for a constant γ.

The results for the $\chi_3 \neq 0$ soliton, calculated using Eq. (5.69) are displayed in tables (6.6)-(6.10) and are also displayed in figure (6.7). There is a subtlety for very small $m_2 << m_1 = \sqrt{8}$ when numerically integrating the differential equation (5.29). The entries of M^2 may differ by two or three orders of magnitude. This causes the upper and lower components of F (which are order $\mathbb{I}$ for $z \rightarrow \infty$) to differ by many orders of magnitude as $z \rightarrow 0$ because the exponential behavior as in Eq. (5.31) for $k = it$ is transferred to $z = 0$ by the separation in Eq. (5.23). In the adaptive step size algorithm, see appendix B, we therefore have to impose very strict accuracy measures that cost quite some CPU-time which is the small value of ϵ in Eq. (B8). In addition we also have to identify a sensible value of z_{max} (representing infinity) for which we obtain numerically stable results.

The general trend is that the ΔE_2 contribution from Eq. (5.61) increases as γ is increased. This is also clearly observed in figure (6.6).

The opposite is true for the E_1 contribution, given by Eq. (5.68), displaying a decrease as γ is increased. We recall that $\Delta E_1 = -\frac{m_2}{\pi}$ equals the VPE of the Sine-Gordon soliton with mass parameter m_2, so that $\Delta E_1 \propto -\sqrt{\gamma}$ for fixed q. For most values of q we observe that the complete VPE decreases as γ increases, which indicates that the decreasing contribution from $2\Delta E_1$ dominates the increase observed for ΔE_2. This

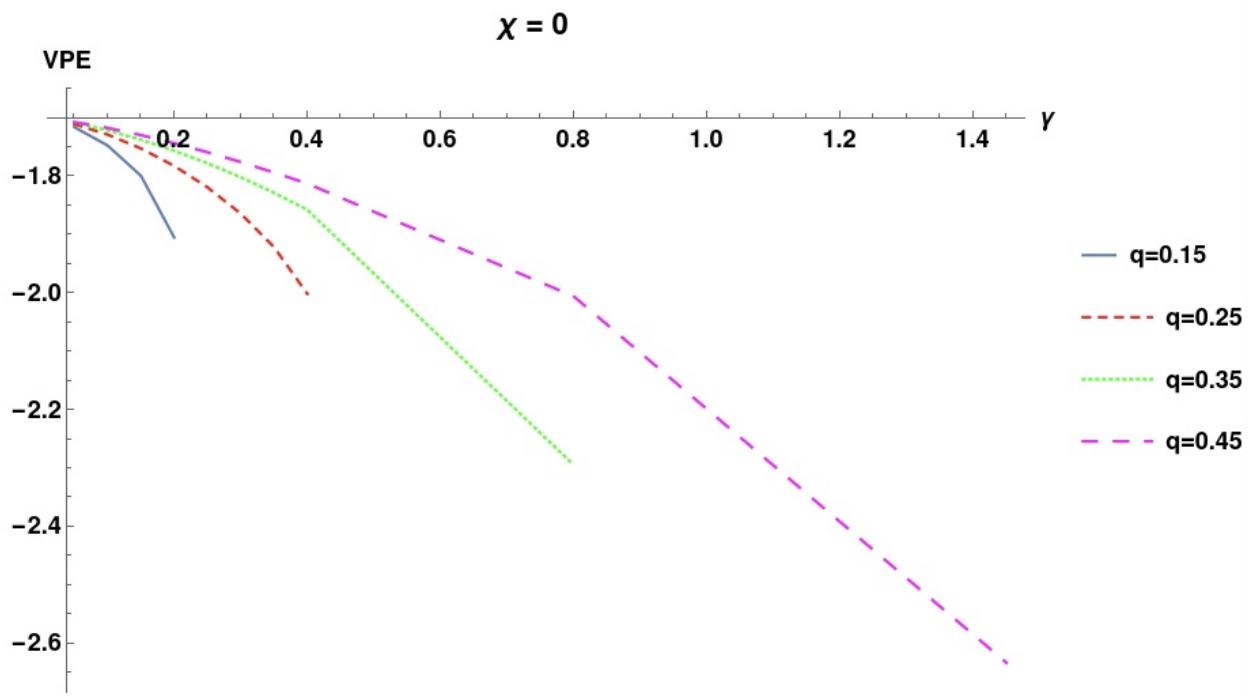

Figure 6.5: $\chi = 0$ VPE results

Table 6.6: $\chi \neq 0$ VPE results for parameters $q = 0.15, \gamma_2 = 0.2076, \mu^2 = 0.85$ and upper γ limit of $\gamma_L = 6.6667$.

γ	0.4	0.5	1.0	1.5	1.7	1.9	2.1	2.3	2.5	6.6
β	7.4×10^{-2}	9.5×10^{-2}	0.21	0.34	0.4	0.47	0.54	0.61	0.70	115.50
ΔE_2	-2.1010	-2.0500	-1.9518	-1.9216	-1.9144	-1.9032	-1.9009	-1.8977	-1.8941	-1.8155
ΔE_1	-0.1103	-0.1233	-0.1743	-0.2135	-0.2272	-0.2402	-0.2525	-0.2642	-0.2755	-0.4478
VPE	-2.3215	-2.2966	-2.3005	-2.3487	-2.3688	-2.3835	-2.4059	-2.4262	-2.4451	-2.7110

does not seem to be the case when $q = 0.45$, due to q being very close to its upper limit of $q < 0.5$, and that the γ values that break the trend are close to the stability limit γ_2. This is also the case for $q = 0.25$ and $q = 0.35$, as seen in the tables (6.7) and (6.8), respectively. The interval $(\gamma_2, \gamma_L) = (1.4876, 2.2222)$ indicates that both the lower and upper boundary cases only leave a small interval for the coupling constant γ.

The boundary case $\gamma = \gamma_2$ is interesting to evaluate. Recall that for $\gamma = \gamma_2$ the two solutions to the stationary field equation are degenerate in energy. Regardless of the loop counting paramater, the VPE will be decisive for establishing the proper soliton solution. We can compute this case numerically by considering the VPE values at $\gamma_2 \pm \epsilon$, where $\epsilon \to 0$. The case $\epsilon \equiv 0$ is numerically tricky because inaccuracies may cause a negative Jost function just above $t = m_2$. Tabulated in table (6.10) are the $\chi_3 = 0$ VPE values calculated with $\gamma - \epsilon$ and the $\chi_3 \neq 0$ VPE values obtained with $\gamma + \epsilon$.

First we note that different intervals of $\gamma \pm \epsilon$ have been used for the two solitons. For the $\chi_3 = 0$ soliton the numerics were uncomplicated due to the case not incorporating the skewed parity and only having one mass parameter in each of the decoupled differential equations. For the $\chi_3 \neq 0$ soliton, $\gamma \to \gamma_2$ resulted in numerical problems explained above. Though we were not able to take ϵ arbitrarily small, we can still

Table 6.7: $\chi \neq 0$ VPE results for parameters $q = 0.25, \gamma_2 = 0.4444, \mu^2 = 0.75$ and upper γ limit of $\gamma_L = 4.0000$.

γ	0.5	0.6	1.0	1.5	1.7	2.1	2.3	2.5	3.99
β	0.07	0.09	0.17	0.30	0.37	0.55	0.68	0.83	199.50
ΔE_2	-1.6176	-1.5249	-1.4057	-1.3190	-1.2912	-1.2406	-1.2172	-1.1946	-1.0433
ΔE_1	-0.1527	-0.1743	-0.2251	-0.2755	-0.2933	-0.3260	-0.3412	-0.3557	-0.4495
VPE	-1.9229	-1.8735	-1.8559	-1.8700	-1.8778	-1.8926	-1.8996	-1.9061	-1.9423

Table 6.8: $\chi \neq 0$ VPE results for parameters $q = 0.35, \gamma_2 = 0.8284, \mu^2 = 0.65$ and upper γ limit of $\gamma_L = 2.8571$.

γ	0.9	1.0	1.2	1.5	1.7	1.9	2.1	2.3	2.5
β	0.10	0.12	0.16	0.24	0.31	0.43	0.59	0.88	1.5
ΔE_2	-1.3241	-1.2794	-1.2195	-1.1538	-1.1171	-1.0835	-1.0521	-1.0223	-0.9938
ΔE_1	-0.2527	-0.2663	-0.2917	-0.3260	-0.3471	-0.3669	-0.3858	-0.4037	-0.4209
VPE	-1.8294	-1.8120	-1.8030	-1.8059	-1.8112	-1.8174	-1.8237	-1.8298	-1.8357

draw a conclusion from the results in table (6.10), where we also list the actual values for $\gamma \approx \gamma_2$. From these values we see that it is only the $q = 0.15$ case for which the $\chi_3 \neq 0$ soliton is favored, since this is the only case where the $\chi_3 \neq 0$ soliton has the smaller VPE. As q is increased, the VPE of the $\chi_3 = 0$ soliton decreases past that of the other soliton. Thus we can conclude that for relatively small q values the $\chi_3 \neq 0$ soliton is favored and the opposite is true when the value of q is increased.

Table 6.9: $\chi \neq 0$ VPE results for parameters $q = 0.45, \gamma_2 = 1.4876, \mu^2 = 0.55$ and upper γ limit of $\gamma_L = 2.2222$.

γ	1.5	1.7	1.9	2.1	2.2
β	0.12	0.18	0.33	0.95	5.50
ΔE_2	-1.3189	-1.2040	-1.1475	-1.1037	-1.0842
ΔE_1	-0.3697	-0.3936	-0.4161	-0.4375	-0.4478
VPE	-2.0583	-1.9911	-1.9798	-1.9786	-1.9798

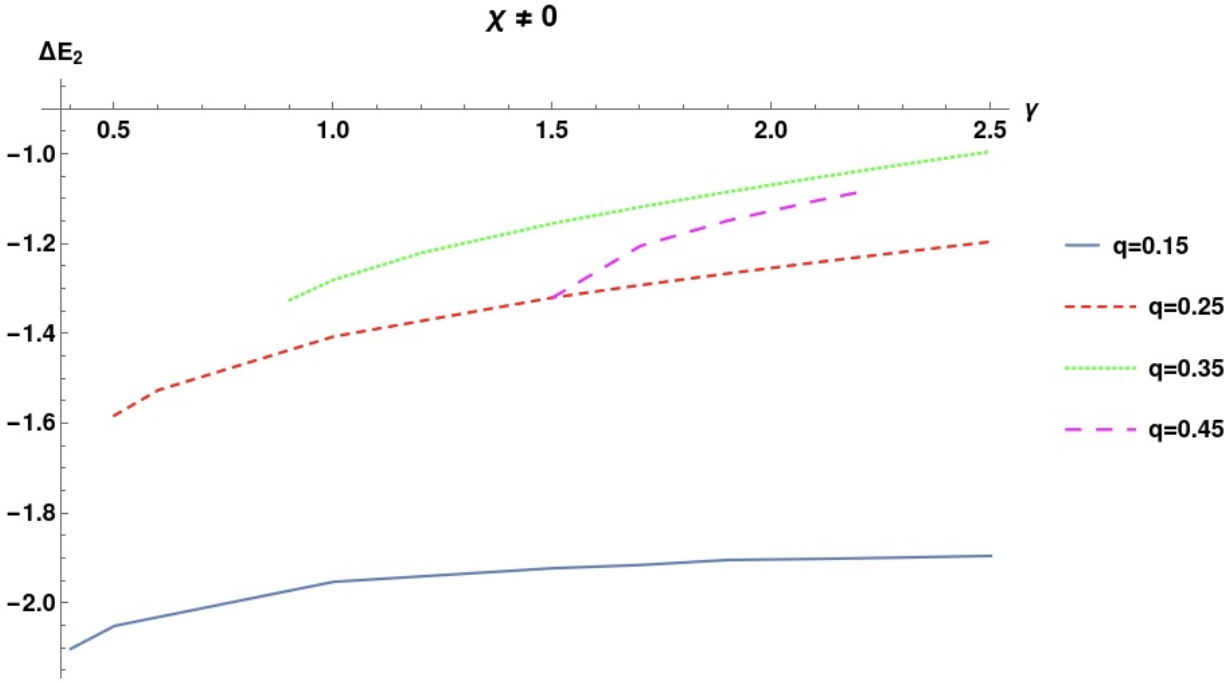

Figure 6.6: ΔE_2 results displaying increasing trend as γ is increased

Table 6.10: Boundary cases $\gamma \approx \gamma_2$ VPE $\chi_3 = 0$ and $\chi_3 \neq 0$

q	γ_2	$\chi_3 = 0$ γ	$\chi_3 = 0$ VPE	$\chi_3 \neq 0$ γ	$\chi_3 \neq 0$ VPE
0.15	0.2076	0.2066	-1.9449	0.3	-2.3710
0.25	0.4444	0.4430	-2.1526	0.5	-1.9229
0.35	0.8284	0.8274	-2.4188	0.9	-1.8294
0.45	1.4876	1.4866	-2.7835	1.5	-2.0583

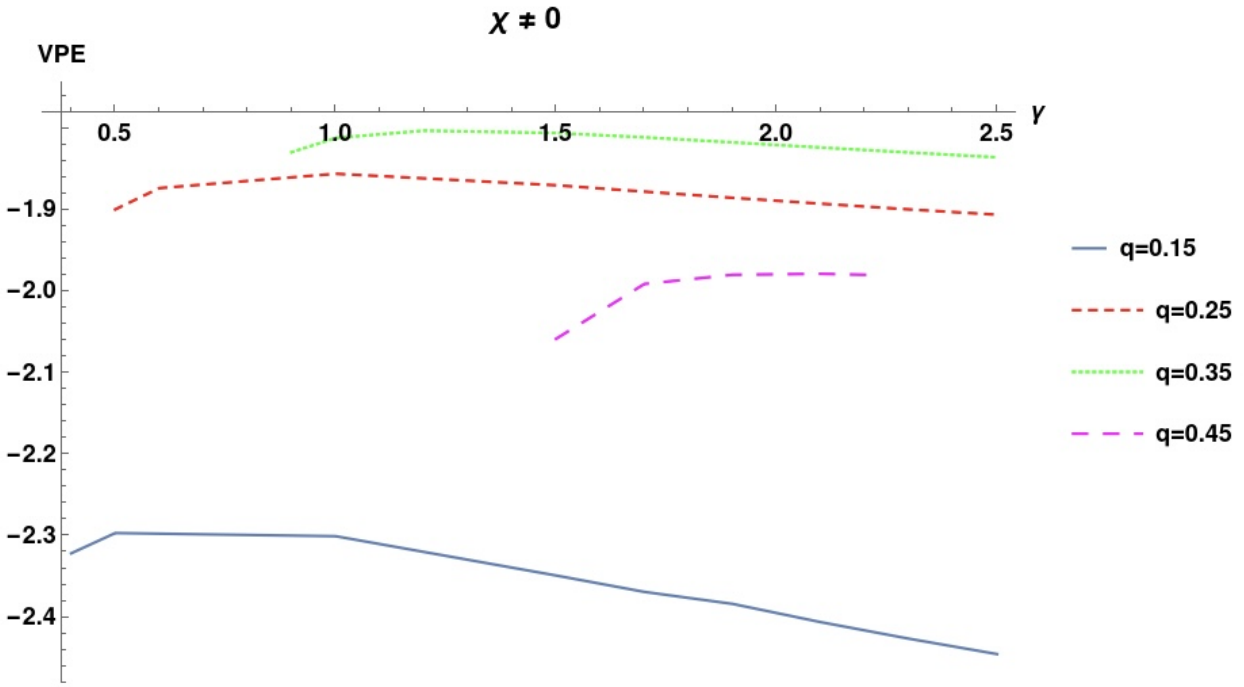

Figure 6.7: $\chi_3 \neq 0$ VPE results: Data displayed in finite intervals bounded by γ_2 and $\frac{1}{q}$, cf. section 5.2.

Chapter 7

Conclusion

In this chapter we will summarize the findings of this thesis and present a short outlook.

We started off considering the classical energy of a soliton in a simple model in one space dimension. We expanded to the vacuum polarization energy (VPE) by means of the spectral method using the analytic properties of the scattering data. Next we considered the sine-Gordon and the ϕ^4 kink solitons and analytically computed the classical energy and the VPE for each. We verified known energies by describing them using the Jost function for both real and imaginary momenta. Following this, we considered the multicomponent model introduced by Gani et al. by also computing the VPE of solitons in this model by means of the Jost function. This required numerical simulations. We performed various numerical tests on these simulations by verifying the known results associated to the sine-Gordon and ϕ^4 kink model to verify the application of these simulations to the multicomponent model. The instability observed by Gani et al. was confirmed and visually illustrated by identifying imaginary energy eigenvalues from the zeros of the Jost functions for the two soliton solutions of the stationary field equations. In this multi-component model, the ϕ^4 theory is augmented by three fields, χ_1, χ_2 and χ_3. One of the solitons only has a non-zero ϕ profile while the other extends to the χ_i components. The analytic solutions are essentially described by two parameters γ and q. The ϕ only soliton ($\vec{\chi} \equiv 0$) is stable for $\gamma < q/(1-q)^2$, as was already shown by Gani et al. We also showed that the other soliton is stable for $\gamma > q/(1-q)^2$. For that soliton we furthermore identify the zero mode associated with rotations amongst the χ_i.

Furthermore we calculated the VPE of both soliton solutions for a variety of q and γ values within their respective regions of stability. For the $\vec{\chi} = 0$ soliton we found that the VPE decreased as γ increased, while q remained constant. We also saw that the VPE decreased as q was increased when γ was kept constant. A similar trend was seen for the $\vec{\chi} \neq 0$ soliton, indicating that the VPE decreased as γ was increased, except when $\gamma \to \gamma_2$.

Finally we considered the situation at the boundary when $\gamma \sim \gamma_2$. We found that for relatively small values of q the $\vec{\chi} \neq 0$ soliton had the smaller VPE, causing it to be the more stable choice. The opposite was true as the value of q was increased, resulting in the $\vec{\chi} = 0$ soliton having the smaller VPE and being the stable case.

Further research on this topic would include the numerical search for alternative solitons outside of the analytical solutions discussed in this thesis. These solutions would not be subject to the constraint of Eq. (5.11). If these solutions are found the VPE should be calculated. While the classical energies do not depend

on the number of components of $\vec{\chi}$, the VPEs do. Hence the generalization from an $SO(3)$ to an $SO(N)$ model is appealing.

Appendices

Appendix A

Runge-Kutta 4^{th} Order Method

In solving our differential equations numerically we are faced with a wide range of options to implement to obtain results [30]. The chosen method is referred to as the fourth order Runge-Kutta method developed in the 1900s by the German mathematicians Carl Runge and Wilhelm Kutta. There exist various Runge-Kutta methods of different orders developed as improvements of the Euler method. Our model contains a second-order ordinary differential equation given by Eq. (5.29) with initial values stated by the boundary conditions. In order to simplify the Runge-Kutta explanation we denote the Jost matrix we wish to solve for as $y = F$ allowing us to rewrite the differential equation as,

$$y'' = 2y'K + [M^2, y] + Vy. \tag{A.1}$$

The initial conditions are given by,

$$\lim_{x\to\infty} y = \mathbb{I} \qquad\qquad \lim_{x\to\infty} y' = 0. \tag{A.2}$$

Any second-order differential equation can be written as two coupled first order equations such that for our case,

$$\frac{dy}{dz} = v \qquad\qquad \frac{dv}{dz} = 2vK + [M^2, y] + V(z)y. \tag{A.3}$$

We introduce $f(v, y, z) = 2vK + [M^2, y] + V(z)y$ and treat the two differential equations simultaneously by evaluating

$$\begin{aligned}
q_1 &= \Delta z v \\
p_1 &= \Delta z f(v, y, z) \\
q_2 &= \Delta z (v + \frac{p_1}{2}) \\
p_2 &= \Delta z f(v + \frac{p_1}{2}, y + \frac{q_1}{2}, z + \frac{\Delta z}{2}) \\
q_3 &= \Delta z (v + \frac{p_2}{2}) \\
p_3 &= \Delta z f(v + \frac{p_2}{2}, y + \frac{q_2}{2}, z + \frac{\Delta z}{2}) \\
q_4 &= \Delta z (v + p_3) \\
p_4 &= \Delta z f(v + p_3, y + q_3, z + \Delta z),
\end{aligned} \tag{A.4}$$

where Δz is the increment of the independent variable. Then the increments of the dependent variables are

$$\Delta y = \frac{1}{6}(q_1 + 2q_2 + 2q_3 + q_4) \tag{A.5}$$

and

$$\Delta v = \frac{1}{6}(p_1 + 2p_2 + 2p_3 + p_4). \tag{A.6}$$

With $v(z) = v$ and $y(z) = y$ the Runge-Kutta theorem thus reads

$$y(z + \Delta z) = y(z) + \Delta y + \mathcal{O}(\Delta z)^5 \tag{A.7}$$

$$v(z + \Delta z) = v(z) + \Delta v\mathcal{O}(\Delta z)^5. \tag{A.8}$$

That is, the algorithm $z \to z + \Delta z, y \to y + \Delta y$ and $v \to v + \Delta v$ produces the correct result up to fourth order in the increment (or step size)

Appendix B

Adaptive Step Size

In order to cut down on computing time we implement an adaptive step size. This automatically adjusts the previously mentioned step size Δz in such a way that it is no longer equi-distant. This will enable us to increase step sizes for smooth parts of the function and alternatively decrease the step size for sections with more erratic behavior.

In particular the increase for the smooth section decreases computing time considerably. The computation consists of two implementations of the Runge-Kuta algorithm from appendix A that we then compare in order to determine whether the step size can be increased or decreased for the next iteration. The first implementation is for a step size $z + 2 \cdot \Delta z$, which is twice the size of the originally stipulated step size. The second consists of a two-step process whereby the independent coordinate is increased to $z + \Delta z$ and then the solution to this computation is used as an input to further increase $z + \Delta z \to z + 2\Delta z$. Introducing the formal operation

$$y(z + \Delta z) = RK[y, z, \Delta z], \tag{B.1}$$

for propagating the function along the interval $[z, z + \Delta z]$ we then introduce

$$y_1 = RK[y, z, 2\Delta z] \tag{B.2}$$

for the single step propagation and

$$y_m = RK[y, z, \Delta z] \tag{B.3}$$

$$y_2 = RK[y_m, z + \Delta z, \Delta z], \tag{B.4}$$

for the two step procedure. We then want the error

$$\Delta_1 = |y_2 - y_1| \tag{B.5}$$

to be less than some prescribed value $\Delta_0 > 0$. Based on the fact that $\Delta_1 \sim \mathcal{O}(\Delta z)^5$, one would update the increment by

$$\Delta z \to \Delta z \left(\frac{\Delta_0}{\Delta_1} \right)^2. \tag{B.6}$$

Experience shows that [30]

$$\Delta z \to \Delta \overline{z} = S \Delta z \begin{cases} (\Delta_0/\Delta_1)^{0.25} & \Delta_0 < \Delta_1 \\ (\Delta_0/\Delta_1)^{0.2} & \Delta_0 > \Delta_1, \end{cases} \tag{B.7}$$

where $S \approx 0.9$ is a safety factor. In the case $\Delta_0 < \Delta_1$ the calculation of z is repeated with the updated Δz. In the other case we use $\Delta\overline{z}$ to propagate form $z + \Delta z$ to $z + \Delta z + \Delta\overline{z}$. There is a local correction based on $y_2 - y_1 \sim \mathcal{O}(\Delta z)^5$ so that $y_2 + \frac{y_2 - y_1}{15}$ equals $y(z + 2\Delta z)$ at order $\mathcal{O}(\Delta z)^6$. A relative error ϵ is prescribed by writing, for example,

$$\Delta_0 = \epsilon[|y(z)| + |E[y(z), 2z]|], \tag{B.8}$$

where E stands for the Euler algorithm operation.

The above explained the adaptive step size control for a single first order differential equation. For multi-components (matrix and/or second order) this algorithm is applied for each component individually.

Appendix C

Numerical Integration

The integrals defined in Eqs. (5.61) and (5.68) require special treatment when considering both the lower and upper bound. The problem with the upper bound (set to ∞) is that it requires the computer to calculate the intergal for an infinite range. Since this is not possible, we set the upper bound to a value that is sufficiently big (t_{max}) and add in an additional term to compensate for the values not taken into account. We know that the integrands in the equations mentioned above fall off as $1/t^3$, and can thus scale the additional term using this factor. Thus the integral is now given by

$$I = \int_{m_2}^{t_{max}} dt \frac{f(t)}{2\pi} + \int_{t_{max}}^{\infty} \frac{dt}{2\pi} \frac{C}{t^3}, \tag{C.1}$$

where $f(t) = \frac{t\nu(t)}{\sqrt{t^2-m_2}}$ and $\nu(t_{max}) = \frac{C}{t^3}$. Solving the integral on the right yields

$$I = \int_{m_2}^{t_{max}} dt \frac{f(t)}{2\pi} + \frac{1}{4\pi} \frac{C}{t_{max}^2} = \int_{m_2}^{t_{max}} dt \frac{f(t)}{2\pi} + \frac{t_{max}}{4\pi} \nu(t_{max}). \tag{C.2}$$

Next we consider the lower bound, which produces a numerical problem for $t = m_2$. To solve the integral numerically we will need to set the lower bound equal to $t = m_2 + \epsilon$, where $\epsilon \to 0$. In doing so we will need to add an additional term to compensate for the integral values leading up to the new lower bound. The integral thus expands to

$$I = \int_{m_2}^{m_2+\epsilon} dt \frac{f(t)}{2\pi} + \int_{m_2+\epsilon}^{t_{max}} dt \frac{f(t)}{2\pi} + \frac{t_{max}}{4\pi} \nu(t_{max}). \tag{C.3}$$

The logarithm of the Jost function is dominated by the zero mode singularity, where the exact calculation is written as $\nu(t) = K \ln(t - m_2)$ where K is the constant to be fitted. Thus we have,

$$I = \frac{1}{2\pi} \int_{m_2}^{m_2+\epsilon} dt \frac{t}{\sqrt{t^2 - m_2^2}} K \ln(t - m_2) + \int_{m_2+\epsilon}^{t_{max}} dt \frac{f(t)}{2\pi} + \frac{t_{max}}{4\pi} \nu(t_{max}). \tag{C.4}$$

When we substitute $t = m_2 + \epsilon$ into $\frac{t}{\sqrt{t^2-m_2^2}}$, which yields $\sqrt{\frac{m_2}{2\epsilon}}$. Using this result we can express K as

$$K = \frac{\sqrt{\frac{2\epsilon}{m_2}}}{\ln \epsilon} f(m_2 + \epsilon). \tag{C.5}$$

Furthermore, when we only consider the first integral in Eq. (C.4), we can simplify it to

$$\begin{aligned} I_1 &= \frac{1}{2\pi}\int_{m_2}^{m_2+\epsilon} \frac{dtt}{\sqrt{t^2-m_2^2}} K\ln(t-m_2) \overset{t=x+m_2}{\approx} \frac{f(m_2+\epsilon)}{2\pi}\int_0^{\epsilon} \frac{dxm_2}{\sqrt{2xm_2}} \frac{\sqrt{\frac{2\epsilon}{m}}}{\ln\epsilon}\ln x \\ &= \frac{1}{\pi}\epsilon\left[1-\frac{2}{\ln\epsilon}\right] f(m_2+\epsilon). \end{aligned} \tag{C.6}$$

Thus considering the top and lower bound additions the full calculation becomes,

$$I = \frac{1}{\pi}\epsilon\left[1-\frac{2}{\ln\epsilon}\right] f(m_2+\epsilon) + \int_{m_2+\epsilon}^{t_{max}} dt\frac{f(t)}{2\pi} + \frac{t_{max}}{4\pi}\nu(t_{max}). \tag{C.7}$$

Lastly, the actual integral is calculated by converting the integral into a differential equation with the boundary conditions exactly solved numerically. The integral thus becomes

$$\frac{dI}{dt} = \frac{f(t)}{2\pi}. \tag{C.8}$$

This differential equation is solved using the Runge-Kutta algorithm with the use of the adaptive step size as explained in appendices A and B respectively.

Bibliography

[1] Itzykson, C. and Zuber, J., 2005. Quantum field theory. Mineola, N. Y.: Dover Publications.

[2] Peskin, M., 2019. Introduction to Quantum Field Theory. CRC Press LLC.

[3] Plato.stanford.edu. 2021. Quantum Field Theory The History of QFT (Stanford Encyclopedia of Philosophy). [online] Available at: https://plato.stanford.edu/entries/quantum-field-theory/qft-history.html.

[4] The quantum theory of the electron. (1928). Proceedings of the Royal Society of London. Series A, Containing Papers of a Mathematical and Physical Character, 117(778), pp.610–624.

[5] Carroll, S. M. [arXiv:2101.07884 [physics.hist-ph]].

[6] Macs.hw.ac.uk. 2021. [online] Available at: https://www.macs.hw.ac.uk/ chris/Scott-Russell/SR37.pdf.

[7] Korteweg, D. J. and de Vries, G., On the change of form of long waves advancing in a rectangular canal, and on a new type of long stationary waves, Phil. Mag. (5) 39 (1895), 422–443.

[8] Brauer, K., 2021. The Korteweg-de Vries Equation: History, exact Solutions, and graphical Representation. [online] Available at: https://www.math.arizona.edu/ gabitov/teaching/141/math485/KDV.pdf.

[9] Sarma, J., 2009. Exact solutions for modified Korteweg–de Vries equation. Chaos, Solitons & Fractals, 42(3), pp.1599-1603.

[10] Rajaraman, R.: Solitons and Instantons: An introduction to solitons and in- stantons in Quantum Field Theory. North Holland, Amsterdam, 1987.

[11] Scott, A.C.: Nonlinear Science: Emergence and Dynamics of Coherent Structure. Oxford: Oxford University Press, 1999.

[12] Sanchez, A. and Bishop, A.: Collective coordinates and length-scale competition in spatially inhomogeneous soliton-bearing equations. *SIAM Rev.*, pp. 579-615, 1998.

[13] Bishop, A., Krumhansl, J. and Trullinger, S.: Solitons in condensed matter: a paradigm. *Physica D*, p. 1, 1980.

[14] Ivanov, B., Kichizhiev, A. and Mitsai, Y.N.: Nonlinear dynamics in relaxation of strongly anisotropic ferromagnets. *Sov. Phys. JETP,* p. 329, 1992.

[15] Anninos, P., Oliveira, S. and Matzner, R.A.: Fractal structure in the scalar $\lambda(\varphi^2 - 1)^2$ theory. *Phys. Rev. D,* p. 1147, 1991.

[16] Bishop, A., Krumhansl, J. and Trullinger, S.: *Solitons in condensed matter: a paradigm.* Berlin: Springer Verlag, 1980.

[17] Witten, E.: Baryons in the 1/N expansion. *Nucl. Phys. B,* p. 57, 1979.

[18] Skyrme, T. H. R., Proc. Roy. Soc. Lond. A **260** (1961), 127-138

[19] Adkins, G. S., Nappi, C. R. and Witten, E., Nucl. Phys. B **228** (1983), 552

[20] Weigel, H.: *Chiral soliton models for baryons,* vol. 743. Berlin: Springer Verlag, 2008.

[21] Gani, V. A., Lizunova, M. A. and Radomskiy, R. V., JHEP **04** (2016), 043 [arXiv:1601.07954 [hep-th]].

[22] Laurell, H: A summary on Solitons in Quantum field theory Available at: http://www.diva-portal.org/smash/get/diva2:935529/FULLTEXT01.pdf

[23] Drozdov, I., [arXiv:hep-th/0311199 [hep-th]].

[24] Graham, N., Quandt, M. and Weigel, H.: Spectral Methods in Quantum Field Theory. Springer, Berlin, Heidelberg, 2009.

[25] Newton, Roger G. Scattering Theory of Waves and Particles . 2nd ed. New York: Springer-Verlag, 1982. Print.

[26] Rebhan, A., Schmitt, A. and van Nieuwenhuizen, P., Phys. Rev. D **80** (2009), 045012 [arXiv:0903.5242 [hep-th]].

[27] Pöschl, G. and Teller, E., Z. Phys. (1933) 143.

[28] Weigel, H. and Graham, N., Phys. Lett. B **783** (2018), 434-439 [arXiv:1806.07584 [hep-th]].

[29] Weigel, H., Quandt, M. and Graham, N., Phys. Rev. D **97** (2018), 036017 [arXiv:1712.04898 [hep-th]].

[30] W. H. Press *et al.*, *Numerical Recipes in Fortran*, Cambridge University Press (1992).